UNIVERSITY OF CALIFORNIA
RIVERSIDE

Development of Stable Gel Polymer and Flame-Resistant Electrolytes Towards Enabling the Assembling of Lithium-ion Batteries Under Open-Air Conditions

A Dissertation submitted in partial satisfaction
of the requirements for the degree of

Doctor of Philosophy

in

Chemical and Environmental Engineering

by

Seungjin Lee

December 2020

Dissertation Committee:
Dr. Alfredo Martinez-Morales, Chairperson
Dr. Juchen Guo
Dr. Boniface Fokwa

The Dissertation of Seungjin Lee is approved:

_____

_____

_____

Committee Chairperson

University of California, Riverside

ABSTRACT OF THE DISSERTATION

Development of Stable Gel Polymer and Flame-Resistant Electrolytes Towards Enabling the Assembling of Lithium-ion Batteries Under Open-Air Conditions

by

Seungjin Lee

Doctor of Philosophy, Graduate Program in Chemical and Environmental Engineering
University of California, Riverside, December 2020
Dr. Martinez-Morales, Chairperson

Driven by the ever-growing energy demand worldwide, lithium-ion batteries (LIBs) continue to be a competitive solution for energy storage systems, ranging from personal electronics to electric vehicles (EVs) and stationary energy storage systems. However, safety continues to be an aspect of high concern and interest for their continued employment and for achieving higher levels of penetration and utilization in the consumer electric market.

The main objectives of this dissertation are focus on the development of: 1) gel polymer electrolytes (GPEs) that can alleviate safety concerns borne from the use of liquid electrolytes, and 2) batteries composed of a titanium-based anode material to enable the assembly of full-cell batteries in open-air conditions. Chapter 1 introduces the background of LIBs, specifically, working principles and their compositions (cathode, anode, separator and electrolyte(s)). Chapter 2 discusses the experimental methods and fundamental theory used throughout this dissertation. Chapter 3, focuses on the design of a full coin-cell and

the selection of components. Specifically, a titanium-based anode material ($Li_4Ti_5O_{12}$, LTO), a lithium transition metal oxide cathode ($LiFePO_4$, LFP), a liquid electrolyte (0.6 m LiBOB), and a gel polymer electrolyte (poly(ethylene glycol) diacrylate (PEGDA)-propylene carbonate (PC)- bis(trifluoromethane)sulfonimide lithium salt (LiTFSI)-lithium bis(oxalato)borate (LiBOB)) are selected based on moisture-resistance and stability in the air criteria needed for the assembly in open-air conditions. Chapter 4 investigates the use of modified GPEs to improve battery characteristics by utilizing high molecular weight polymer host, poly(ethylene oxide) (PEO), or lithium salt additives (LiTFSI, LiBOB) to: 1) strengthen mechanical properties, and 2) to improve the interfacial stability between electrolyte and electrodes. From the study and analysis of battery performance tests, it is concluded that the PEO-based GPEs composed of LiBOB without LiTFSI shows significantly improved stable cyclic performance, compared to PEGDA-based GPE. Also, the thermal stability, glass transition temperature, and crystallinity of GPEs are evaluated by Thermogravimetric (TGA) analysis, Differential Scanning Calorimetry (DSC), and X-ray Powder Diffraction (XRD), as well as the study of electrochemical characterizations such as Cyclic Voltammetry (CV), Linear Sweep Voltammetry (LSV), and Electrochemical Impedance Spectroscopy (EIS). The battery performance such as charging and discharging profiles and cycling performance are investigated by using CR2032 coin-cell composed of LFP/GPE/LTO configuration. In addition to the physical and electrochemical characterization, Chapter 3 and Chapter 4, present and discuss the results from flammability tests during electrolyte development. Lastly, the conclusion and remarks are summarized in Chapter 5.

Table of Contents

CHAPTER 1. INTRODUCTION 1
1.1 Background and Motivation 1
1.2 Principle of Lithium-ion Batteries 2
1.3 Cathode and Anode Materials 4
1.3.1 Cathode Materials 4
1.3.2 Anode Materials 6
1.4 Electrolytes 7
1.4.1 Organic Carbonate-based Electrolytes 7
1.4.2 Conducting Salts 8
1.4.2.1 Lithium hexafluorophosphate ($LiPF_6$) 8
1.4.3 Polymer Electrolytes 11
1.5 Scope of the Dissertation 13
Reference 1
CHAPTER 2. EXPERIMENTAL METHODS AND THEORY 1
2.1 Chemical and Materials 1
2.2 Equipment for Measurements 1
2.2.1 Morphology and Structural Analysis 1
2.2.2 Electrochemical Analysis 2
2.3 Cell Preparation 2
2.3.1 Electrode Preparation 2
2.3.2 Electrolyte Preparation 5
2.3.3 Cell assembly 7
2.4 Fundamental Background Theory 9
2.4.1 Thermogravimetric Analysis (TGA) 9
2.4.2 Differential Scanning Calorimetry (DSC) 10
2.4.3 X-ray diffraction (XRD) Analysis 11
2.5 Electrochemical Characterization 11
2.5.1 Cyclic Voltammetry (CV) 11

2.5.2 Linear Sweep Voltammetry (LSV) 13
2.5.3 Electrochemical Impedance Spectroscopy (EIS) 14
2.5.4 Ionic Conductivity 16
2.5.5 Battery Performance 17
Reference 18
CHAPTER 3. DEVELOPMENT OF A GEL POLYMER ELECTROLYTE FOR A SAFE FULL CELL 19
3.1 Introduction 19
3.2 Experimental 23
3.2.1 Gel Polymer Electrolyte Preparation 23
3.2.2 Thermal Analysis of GPE 24
3.2.3 SEM, XRD and FT-IR Characterization 24
3.2.4 Electrodes Preparation and Full-cell Fabrication 24
3.2.5 Electrochemical Characterization 25
3.3 Results and Discussion 26
3.3.1 Material Properties 26
3.3.2 Electrochemical Properties 31
3.3.3 Flammability Test 37
3.4 Conclusion 39
Reference 41
CHAPTER 4. MODIFICATION OF THE GEL POLYMER ELECTROLYTE FOR THE SAFE FULL CELL 45
4.1 Introduction 45
4.2. Experimental 49
4.2.1 Electrolyte Preparation 49
4.2.2 GPE Characterizations 51
4.2.3 Electrochemical Characterization 51
4.3. Results and Discussion 52
4.3.1 Material Properties 52

4.3.2 Electrochemical Properties 56
4.4 Conclusion 65
Reference 66
CHAPTER 5. CONCLUSION 69

List of Figures

Figure 1. 1 Schematic diagram of a lithium-ion battery 4
Figure 1. 2 The potential range of common electrode materials 7
Figure 1. 3 Chemical structure of $LiPF_6$ 9
Figure 1. 4 Chemical structure of LiTFSI 10
Figure 1. 5 Chemical structure of LiBOB 11
Figure 2. 1 Electrode preparation for LFP casted on the Al foil (left) and LTO casted on the Cu foil (right) 3
Figure 2. 2 SEM images of a) LFP surface and b) LTO surface 4
Figure 2. 3 A preparation procedure for the GPEs 6
Figure 2. 4 PEO-based GPE electrolyte on the LFP electrode and CR2032 case 7
Figure 2. 5 Schematic image of CR2032 coin-cell assembly for liquid electrolyte (left) and GPE electrolytes (right) 8
Figure 2. 6 TGA curve for GPE-C1(60/10/30) 9
Figure 2. 7 DSC curve for GPE-C1(60/10/30) 10
Figure 2. 8 Cyclic voltammogram [5] 13
Figure 2. 9 LSV of the PEO-based gel polymer electrolyte at 0.5 mV/s [6] 14
Figure 2. 10 Nyquist plot for mixed kinetic and diffusion system 15
Figure 2. 11 Typical Nyquist plot with two semi-circles and a Warburg 16
Figure 3. 1 TGA thermogram of (a) the precursors and (b) GPEs prepared in different composition 27
Figure 3. 2 DSC thermograms of precursors and GPEs 28
Figure 3. 3 XRD patterns of precursors and GPEs prepared in different composition 30
Figure 3. 4 Nyquist plots for GPEs with different formulations 31
Figure 3. 5 CV for GPEs with different composition in (a) C1(60/10/30) (b) C2(50/20/30), and (c) C3(40/30/30/) 33
Figure 3. 6 CV for GPEs with different composition in (d) C4(30/40/30) (e) C5(20/50/30), and (f) C6(10/60/30/) 34
Figure 3. 7 LSV curve for LFP/GPE/LTO cell with C1 34

Figure 3. 8 1st cycle of (a) charging and (b) discharging of GPEs..... 36
Figure 3. 9 Cycling performance for GPEs 37
Figure 3. 10 Flammability test for GPEs 38
Figure 3. 11 Flammability test for PC and PEGDA 38
Figure 4. 1 Illustration of the different electrolytes in LIBs [8] 46
Figure 4. 2 Chemical structures of the GPE components: PEO, PC, LiTFSI and LiBOB 50
Figure 4. 3 TGA thermogram of a) the precursors and GPEs prepared with b) 1 M LiTFSI-LiBOB, c) 0.5 M LiTFSI-LiBOB, and d) 0.5 M LiBOB-LiTFSI compositions . 53
Figure 4. 4 DSC thermograms of a) the precursors and GPEs prepared with b) 1 M LiTFSI-LiBOB, c) 0.5 M LiTFSI-LiBOB, and d) 0.5 M LiBOB-LiTFSI compositions . 54
Figure 4. 5 XRD patterns of precursors and GPEs prepared in different composition 56
Figure 4. 6 Nyquist plots for GPEs with different formulations..... 57
Figure 4. 7 First 3 cycles for GPEs with 1 M LiTFSI composition..... 59
Figure 4. 8 First 3 cycles for GPEs with 0.5 M LiTFSI composition..... 60
Figure 4. 9 First 3 cycles for GPEs with 0.5 M LiBOB composition..... 60
Figure 4. 10 Charge and discharge profile for the 1st cycle of GPEs..... 62
Figure 4. 11 Cycling performance of GPEs..... 64

List of Tables

Table 1. 1 List of organic solvents for lithium battery electrolytes [36] 8
Table 3. 1 Different composition for GPEs 23
Table 3. 2 Room temperature ionic conductivity for different GPE formulations 32
Table 4. 1 Different composition for GPEs 50
Table 4. 2 Room temperature ionic conductivity for different GPE formulations 58

CHAPTER 1. INTRODUCTION

1.1 Background and Motivation

Since their commercialization by Sony in 1991, LIBs have been dramatically improved for 25 years. Owing to their high energy density and long cycle life, LIBs have been widely employed in portable electronics. [1–4] However, the safety of LIBs has become an increasingly important and urgent matter over the years. [5] The risk of explosion in commercial LIBs results both from the highly reactive and flammable battery cell components, mainly the electrodes and liquid electrolytes used. Specifically, the liquid electrolyte is the most ignitable component inside the battery and can lead to many exothermic reactions that produce heat within the cell. [6, 7] An increasing need for safer electrolytes is become urgent, as new cathode and anode materials with higher energy density are developed. [8–10] Enhancing the electrolyte safety is one of the most important and effective ways to reduce the thermal risk of the next generation of LIBs. [11]

To address the safety issue of LIBs, solid-state (polymer or inorganic) electrolytes have attracted researchers' interests since replacing the organic electrolyte is a direct and effective way to addressing safety concerns. [12] Especially, gel polymer electrolytes (GPEs) have been considered as a potential candidate for preventing potential safety issues such as leaks, flammability, and toxicity due to their mechanical robustness. The use of an organic solvent plasticizer in GPEs decreases the crystallinity of the polymer, which leads to a higher ionic conductivity that results from increasing the polymer's amorphousness.

[13] GPEs can achieve higher ionic conductivity, while maintaining mechanical integrity and safety, because the ion-transport in GPEs generally occurs in the liquid phase of the organic solvent within the polymer matrix that supports the physical structure of GPEs. As such, Li^+ transport is facilitated by a segment chain motion of polymer in a solid polymer electrolyte. [14] However, increasing the amorphousness of a polymer is associated with a decrease in the mechanical stability of the system, as the crystalline domains are responsible for the resistance towards deformation in the polymer. [15] Thus, it is essential to find the optimized combination between plasticizer and polymer host that are suitable for GPEs applications.

Besides improving the electrolyte, selecting chemically stable electrodes is an important factor to develop safer batteries. Researchers have paid attention to LFP and LTO as cathode and anode material, respectively, because of their long cycle life, excellent safety and stability, especially for stationary energy storage applications. [16, 17] Herein, we develop a facile synthesis method for gel polymer electrolytes using lithium salts such as LiTFSI and LiBOB, in combination with LFP and LTO electrodes. The developed method permits the assembly of a full cell battery that can endure complete exposure to the open-air environment during fabrication.

1.2 Principle of Lithium-ion Batteries

The basic working principle of LIBs is based on the reversible intercalation and de-intercalation of lithium ions, Li^+ into the electrodes. [18] During charging, electrons generated from the oxidation of cathode move from the cathode to anode through an

external circuit, while the Li^+ travel simultaneously to the anode through the electrolyte for the reduction of lithium ions. These transportation and redox reactions between electrons and Li^+ reversely take place for discharging. The entire reaction mechanism of LIB is shown in Figure 1.1. This flow converts chemical energy into electrical energy, and in its opposite reaction enables the storage of electrochemical energy within the battery. [19]

Typical electrochemical cells are composed of several complex components. For instance, they include metal current collectors, a cathode and anode that consist of active materials such as $LiCoO_2$ (LCO) and graphite, respectively. The electrodes are prepared by casting on the current collectors from a slurry containing polymer binders such as poly(vinylidene fluoride) (PVDF), conductive carbons (Super P) and N-Methyl-2-Pyrrolidone (NMP) as solvents. The electrodes are isolated by a separator film (microporous poly(ethylene)), which is embedded with the electrolyte. Additionally, a solid electrolyte interface (SEI) layer is formed by a reaction between the electrode and electrolyte on the surface of the electrodes during the first cycle. The battery cycle life is dependent on the quality of the SEI layer. The voltage, capacity, specific energy, and power density are determined by the selection of electrodes. [18]

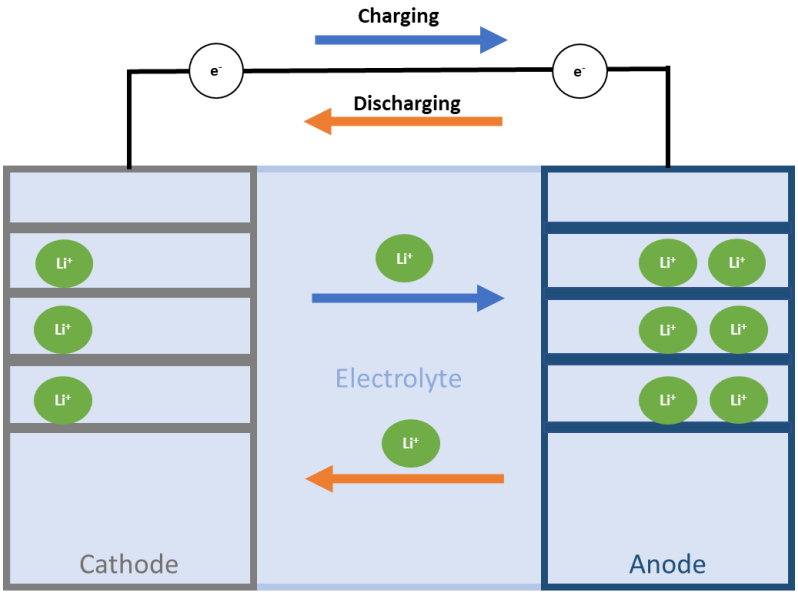

Figure 1. 1 Schematic diagram of a lithium-ion battery

1.3 Cathode and Anode Materials

1.3.1 Cathode Materials

LCO has been used for the conventional C/LCO cell since the first rechargeable LIBs were developed by Sony in 1991. The charging voltage of LCO is limited to < 4.2 V vs. Li/Li^+ and its theoretical capacity is about 274 mAh/g. However, if more than half of the lithium leaves the crystal, the structure may collapse and liberate oxygen. [20] This can cause thermal runaway, as oxygen is able to burn the electrolyte. Therefore, only 50% of the lithium may be utilized, leading to the maximum capacity of 140 to 150 mAh/g. Due to its low thermal stability, high cost and environmental impacts of Co, research has been mostly focused to lower cost and toxicity than LCO. [21]

$LiNi_{0.33}Mn_{0.33}Co_{0.33}O_2$ (NMC) has efficiently replaced LCO with a lower Co content, an average operating voltage of about 3.7 V vs. Li/Li^+, higher reversible capacity (about 180-185 mAh/g) and higher thermal stability in its delithiated form. [22] However, NMC still exhibit an excessively high irreversible capacity due to the mixed population on the lithium position. [23] $Li_{1-x}Mn_2O_4$ (LMO spinel) has the advantage of high manganese content, resulting in environmentally safe and a discharge voltage of around 4.0 V vs Li/Li^+. However, LMO exhibits low theoretical capacity of 110 mAh/g, poor cycling performance and rapid capacity fading at temperatures above 50 ℃. [22]

LFP with an olivine structure is a low cost and environmentally friendly cathode material already commercialized in LIBs even though its energy density and operation voltage are lower than LCO. LFP shows remarkable chemical and electrochemical stability with the theoretical capacity of 170 mAh/g and an operating voltage around 3.4 V vs Li/Li^+. [24] Moreover, LFP is relatively inexpensive electrode material (USD 0.1235 kg^{-1}, as of September 2020; www.dailymetalprice.com) since iron is an abundant Earth element. [25] However, the poor electrical and lithium-ion conductivity can lead to poor cell performance, so that the conductive layer coating is required. [26]

1.3.2 Anode Materials

Graphite is one of the most used anode materials where the electrochemical intercalation of non-solvated lithium occurs within a potential range of 0 to 0.25 V vs Li/Li^+. Graphite has a theoretical specific capacity of 370 mAh/g. However, it has almost achieved the theoretical capacity of graphite. [27]

Lithium metal has a low density (0.534 g/cm^3) and the lowest negative electrochemical potential (-3.040 V versus standard hydrogen electrode), resulting in very high specific capacity (3,860 mAh/g) and high cell voltage. [28] However, cycling efficiency decreases as lithium dissolves repeatedly and forms lithium dendrites during charging and discharging. Lithium dendrites over time lead to the internal short circuit between the electrodes, which results in a thermal chain reaction, fire, or explosion. [29, 30]

The replacement of lithium metal with a lithium storage medium to produce safe cells with a good cycling efficiency has been widely investigated. [31] Lithium titanate (LTO) and titanium oxide (TO) are promising as anode active materials for improving cycling stability with high power and safety characteristics. TO reversibly intercalates lithium at 1.55 V (vs. Li/Li^+) and LTO reaches a reversible capacity of around 160 mAh/g. Also, there are other advantages such as no SEI formation, low internal resistance, good cycling stability, and safety. [32] Therefore, LTO is especially suitable for large cells in stationary applications or for cells in areas with high power requirements (e.g., hybrid vehicles). [33]

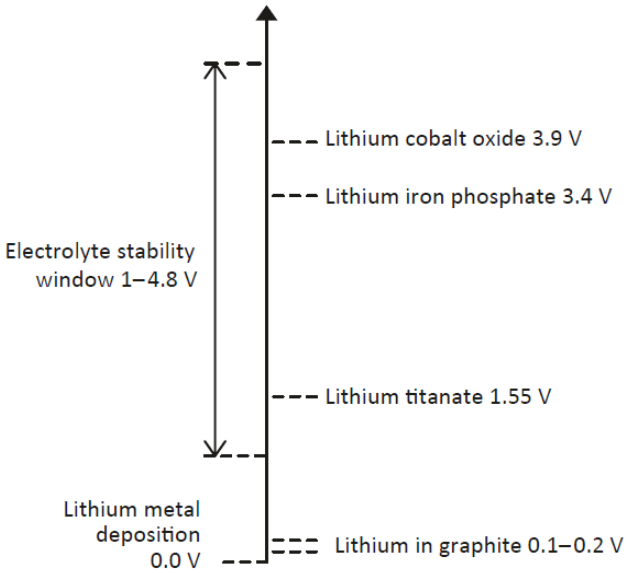

Figure 1. 2 The potential range of common electrode materials [34]

1.4 Electrolytes

1.4.1 Organic Carbonate-based Electrolytes

State-of-the-art electrolyte solvents usually use a mixture of organic carbonates, which are cyclic and linear carbonates. Ethylene carbonate (EC) and propylene carbonate (PC) are the most used cyclic carbonates that possess high dielectric constants (ε, EC = 89.78, PC = 64.92). Dimethyl carbonate (DMC), diethyl carbonate (DEC), ethyl methyl carbonates (EMC) are the linear carbonates which provide low viscosities (η, DMC = 0.59, DEC = 0.75, EMC = 0.65), and thus, contribute to a suitable ionic conductivity by lowering the overall viscosity of the mixture.[6] However, these carbonate solvent mixtures such as EC (flash point: 160 ℃), DMC (flash point: 18 ℃), and (EC and DMC mixture: flash point:

23 °C) are highly volatile and possess low thermal stability in the presence of lithium salt, causing serious safety concerns. [35]

Table 1. 1 List of organic solvents for lithium battery electrolytes [36]

Solvent	T_m/°C	η/cP, 25 °C	ε, 25 °C	ρ/gcm^{-3}, 25 °C
EC	36.4	1.9	89.78	1.321
PC	-48.8	2.53	64.92	1.2
DMC	4.6	0.59	3.107	1.063
DEC	-74.3	0.75	2.805	0.969
EMC	-53	0.65	2.958	1.006

1.4.2 Conducting Salts

1.4.2.1 Lithium hexafluorophosphate ($LiPF_6$)

$LiPF_6$ is the most widely used lithium salt in commercial lithium-ion batteries due to its high conductivity of 8 to 12 mS/cm at RT and electrochemical stability up to almost 5 V (vs. Li/Li^+). Also, $LiPF_6$ effectively prevents the corrosion of the aluminum current collector that take places at potentials above 3 V (vs. Li/Li^+) in the positive electrode. However, $LiPF_6$ over time disintegrates into lithium fluoride (LiF) and phosphorus pentafluoride (PF_5).

$$LiPF_6 \leftrightarrow LiF(s) + PF_5(g)$$

At temperatures above 70 °C $LiPF_6$ disintegrates and reacts with small amounts of water, forming hydrofluoric acid (HF). [37]

$$LiPF_6 + H_2O \rightarrow LiF + 2HF + POF_3$$

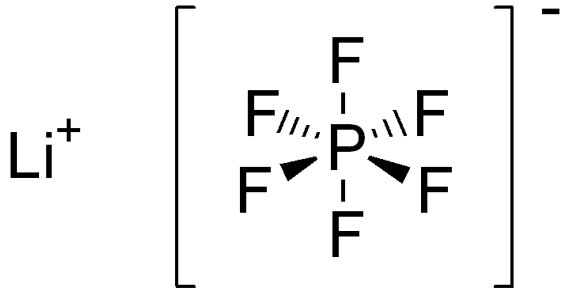

Figure 1. 3 Chemical structure of $LiPF_6$

1.4.2.2 Lithium-bis(trifluorosulfonyl)imide (LiTFSI)

There have been efforts to replace $LiPF_6$ because it is highly susceptible to hydrolysis. The most promising approach uses compounds that are based on sulfonylimides, for instance lithium-bis(trifluorosulfonyl)imide. The $TFSI^-$ anion provides high chemical stability towards all cell components as it has low Lewis acidity due to the delocalized negative charge, which results in superior electrochemical stability towards oxidation. [38, 39] LiTFSI exhibits a high conductivity of 12 mS/cm at RT, which is higher than that of $LiPF_6$, making it suitable for high-current applications. LiTFSI also demonstrates hydrolysis-resistance and high thermal stability, requiring more than 200 ℃ to degrade. However, there are major drawbacks of LiTFSI. It is observed that the corrosion of the aluminum conductors on the cathode is an issue caused by an insufficient or the lack of a potential-stable formation of a passivation layer at around 3.7 V. [40, 41]

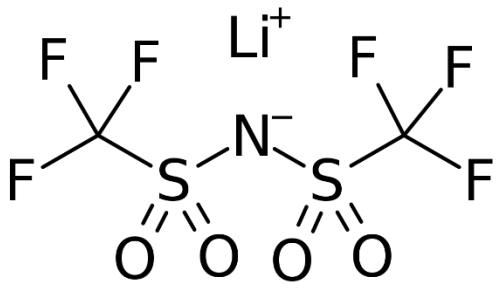

Figure 1. 4 Chemical structure of LiTFSI

1.4.2.3 Lithium-bis(oxalate)borate (LiBOB)

Chelatoborates were developed to replace conventional salts with environmentally friendly conducting salts. Among chelatoborates, LiBOB is the most successful variant with boron as the central atom as a non-toxic, non-corrosive conducting salt for specific applications. LiBOB can be used as an additive to form extraordinary film on the electrode. The film formation characteristics are observed on both the anode and the cathodic current collector foil. This is because $AlBO_3$ is typically produced on the surface passivation when LiBOB degrades, which is stable enough to withstand potentials of up to 5 V. As a result, additives such as LiBOB that form a passivation layer achieve a significant increase in service life. However, there are several disadvantages of LiBOB. It exhibits moderate conductivity 6-7 mS/cm at RT. Considering LiBOB as an additive only, it is susceptible to hydrolysis, and can lead to the development of gas during the forming of the cell. [42, 43]

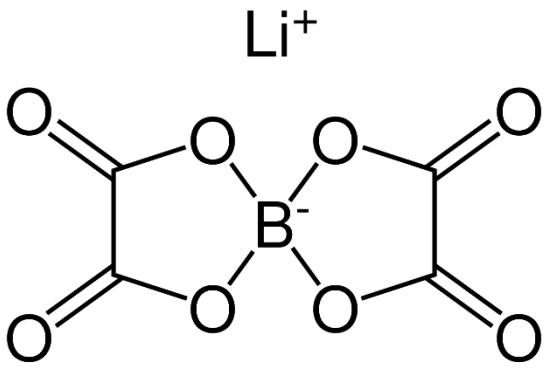

Figure 1. 5 Chemical structure of LiBOB

1.4.3 Polymer Electrolytes

Polymer electrolytes for solid-state LIBs have been considered as a promising prospect for the enhancement of safety, long-term stability, and flexibility of electrolytes. These electrolytes can be classified into two categories: solid polymer electrolytes and gel polymer electrolytes.

1.4.3.1. Solid Polymer Electrolytes (SPEs)

SPEs have been continuously researched to develop a safer lithium-ion battery because in addition to high mechanical stability and flexibility, they do not contain flammable liquid state organic solvents. [44] PEO-based polymer electrolytes have attracted attention owing to their excellent salt-dissolving ability, availability at various molecular weight, and mechanical stability. [45] The transport of lithium-ion is coordinated by the corresponding anions and ether oxygen atoms and lithium-ion conduction results principally from two

phenomena: 1) the hopping of lithium ions along the polymer chain and 2) the segmental motion of the polymer chain itself. [46] The overall lithium-ion conductivity relies on the molecular weight of the polymer (i.e., a higher molecular weight results in less segmental motion, and thus, lower conductivity) and the nature of the lithium salt anion. [47] PEO with LiTFSI polymer electrolytes show a high lithium-ion transference number because of its large anion. [48] Nevertheless, the ionic conductivity of SPEs at RT is usually in the range of 10^{-8} to 10^{-4} S/cm. Thus, it is important to improve the ionic conductivity without compromising the mechanical robustness.

1.4.3.2. Gel Polymer Electrolytes (GPEs)

Quasi-solid-state electrolytes resulting from combining a polymer and organic liquid electrolyte have been introduced to increase the ionic conductivity of polymer electrolytes. [37, 38] The organic solvents such as EC, PC, DEC, DMC are often referred to the common ester carbonate solvents. Ionic liquids can be used as the organic solvents due to their low flammability and high safety. Since the polymer matrix traps the organic solvents, it enhances the ionic conductivity and the loss of mechanical strength. Because these two-phase solid electrolytes combine the advantageous mechanical properties of the polymer with the chemical and electrochemical properties of liquid organic electrolytes, the ionic conductivity of polymer electrolyte can be as high as 10^{-4}-10^{-3} S cm^{-1}. It is generally called a gel polymer electrolyte due to its plastic properties, with organic solvents used as plasticizers. [51]

The plasticizers such as EC and PC improve the ionic conductivity up to 10^{-3} S cm^{-1}, while decreasing the mechanical strength significantly. [13, 52] To overcome the weakened mechanical strength, UV cross-linking can be used as a method to improve the mechanical stability of PEO. [53] Alternatively, PEO can be blended with another polymer such as PVDF because of its good mechanical strength. However, PVDF alone is not proper to be used as a polymer matrix because PVDF is highly crystalline and results in a low ionic conductivity. [54]

1.5 Scope of the Dissertation

The goal of this dissertation is to develop gel polymer electrolytes for enhancing the safety aspects of battery assembled in the open-air environtment. The electrodes are selected based on their chemical and environmental stability, non-toxicity, and stability to moisture. The electrolyte and electrodes are prepared under complete ambient conditions. The details are discussed in the following chapters.

In chapter 2, the synthesis process of electrodes, GPEs and coin-cell preparation, including electrochemical and characterization techniques used in the work are discussed. In chapter 3, GPEs are prepared in ambient conditions, using oligomer polymer host, plasticizer and dual lithium salts to improve ionic conductivity and safety at RT. Coin-cells based on LIB are assembled in ambient condition using GPE and their battery performance is tested. In chapter 4, the mechanical properties of GPEs are enhanced by adding higher molecular polymer to improve the cyclic performance of full cells. In addition, the electrochemical

characteristics are carried out to understand the mechanism of their properties. Chapter 5 discusses the conclusion of the dissertation.

Reference

[1] A. J. Bard and L. R. Faulkner, *Fundamentals and Applications*, vol. 30. 1980.

[2] M. L. Heilig, "United States Patent Office," *ACM SIGGRAPH Comput. Graph.*, vol. 28, no. 2, pp. 131–134, 1994, doi: 10.1145/178951.178972.

[3] Yoshino, "Secondary battery, US patent 4668595A," *United States Pat.*, no. 19, p. 9, 1987, [Online]. Available: https://pubs.acs.org/doi/10.1021/acsnano.7b04646.

[4] T. Fujita and K. Toda, "Microdisplacement measurement using a liquid-delay-line oscillator," *Japanese J. Appl. Physics, Part 1 Regul. Pap. Short Notes Rev. Pap.*, vol. 42, no. 9 B, pp. 6131–6134, 2003, doi: 10.1143/jjap.42.6131.

[5] B. Scrosati, J. Hassoun, and Y. K. Sun, "Lithium-ion batteries. A look into the future," *Energy Environ. Sci.*, vol. 4, no. 9, pp. 3287–3295, 2011, doi: 10.1039/c1ee01388b.

[6] J. Kalhoff, G. G. Eshetu, D. Bresser, and S. Passerini, "Safer electrolytes for lithium-ion batteries: State of the art and perspectives," *ChemSusChem*, vol. 8, no. 13, pp. 2154–2175, 2015, doi: 10.1002/cssc.201500284.

[7] M. Marcinek *et al.*, "Electrolytes for Li-ion transport - Review," *Solid State Ionics*, vol. 276, pp. 107–126, 2015, doi: 10.1016/j.ssi.2015.02.006.

[8] J. Wang *et al.*, "Fabrication of an anode composed of a N, S co-doped carbon nanotube hollow architecture with CoS2 confined within: Toward Li and Na storage," *Nanoscale*, vol. 11, no. 43, pp. 20996–21007, 2019, doi: 10.1039/c9nr07767g.

[9] M. Ko *et al.*, "Scalable synthesis of silicon-nanolayer-embedded graphite for high-energy lithium-ion batteries," *Nat. Energy*, vol. 1, no. 9, pp. 1–8, 2016, doi: 10.1038/nenergy.2016.113.

[10] Y. K. Sun, S. T. Myung, B. C. Park, J. Prakash, I. Belharouak, and K. Amine, "High-energy cathode material for long-life and safe lithium batteries," *Nat. Mater.*, vol. 8, no. 4, pp. 320–324, 2009, doi: 10.1038/nmat2418.

[11] X. Cao *et al.*, "High Voltage LiNi0.5Mn1.5O4/Li4Ti5O12 Lithium Ion Cells at Elevated Temperatures: Carbonate- versus Ionic Liquid-Based Electrolytes," *ACS Appl. Mater. Interfaces*, vol. 8, no. 39, pp. 25971–25978, 2016, doi: 10.1021/acsami.6b07687.

[12] Z. Xue, D. He, and X. Xie, "Poly(ethylene oxide)-based electrolytes for lithium-ion batteries," *J. Mater. Chem. A*, vol. 3, no. 38, pp. 19218–19253, 2015, doi:

10.1039/c5ta03471j.

[13] H. M. J. C. Pitawala, M. A. K. L. Dissanayake, V. A. Seneviratne, B. E. Mellander, and I. Albinson, "Effect of plasticizers (EC or PC) on the ionic conductivity and thermal properties of the (PEO) 9LiTf: Al 2O 3 nanocomposite polymer electrolyte system," *J. Solid State Electrochem.*, vol. 12, no. 7–8, pp. 783–789, 2008, doi: 10.1007/s10008-008-0505-7.

[14] L. Long, S. Wang, M. Xiao, and Y. Meng, "Polymer electrolytes for lithium polymer batteries," *J. Mater. Chem. A*, vol. 4, no. 26, pp. 10038–10039, 2016, doi: 10.1039/c6ta02621d.

[15] Y. Lu, Y. Cai, Q. Zhang, L. Liu, Z. Niu, and J. Chen, "A compatible anode/succinonitrile-based electrolyte interface in all-solid-state Na-CO2 batteries," *Chem. Sci.*, vol. 10, no. 15, pp. 4306–4312, 2019, doi: 10.1039/c8sc05178j.

[16] D. Choi *et al.*, "Li-ion batteries from LiFePO4 cathode and anatase/graphene composite anode for stationary energy storage," *Electrochem. commun.*, vol. 12, no. 3, pp. 378–381, 2010, doi: 10.1016/j.elecom.2009.12.039.

[17] D. C. T. Xu, W. Wang, M.L. Gordin, D. Wang, "2010_Xu,Wang,Choi-LIB for stationary energy storage.pdf." p. 62, 2010.

[18] M. S. Balogun *et al.*, "A review of the development of full cell lithium-ion batteries: The impact of nanostructured anode materials," *Nano Res.*, vol. 9, no. 10, pp. 2823–2851, 2016, doi: 10.1007/s12274-016-1171-1.

[19] A. Manthiram and C. Tsang, "Electrode materials for rechargeable lithium batteries," *An. des la Asoc. Quim. Argentina*, vol. 84, no. 3, pp. 265–270, 1996.

[20] J. Li, Q. Zhang, X. Xiao, Y. T. Cheng, C. Liang, and N. J. Dudney, "Unravelling the Impact of Reaction Paths on Mechanical Degradation of Intercalation Cathodes for Lithium-Ion Batteries," *J. Am. Chem. Soc.*, vol. 137, no. 43, pp. 13732–13735, 2015, doi: 10.1021/jacs.5b06178.

[21] D. Di Lecce, R. Verrelli, and J. Hassoun, "Lithium-ion batteries for sustainable energy storage: Recent advances towards new cell configurations," *Green Chem.*, vol. 19, no. 15, pp. 3442–3467, 2017, doi: 10.1039/c7gc01328k.

[22] P. Rozier and J. M. Tarascon, "Review—Li-Rich Layered Oxide Cathodes for Next-Generation Li-Ion Batteries: Chances and Challenges," *J. Electrochem. Soc.*, vol. 162, no. 14, pp. A2490–A2499, 2015, doi: 10.1149/2.0111514jes.

[23] O. Dolotko, A. Senyshyn, M. J. Mühlbauer, K. Nikolowski, and H. Ehrenberg,

"Understanding structural changes in NMC Li-ion cells by in situ neutron diffraction," *J. Power Sources*, vol. 255, pp. 197–203, 2014, doi: 10.1016/j.jpowsour.2014.01.010.

[24] J. Wang and X. Sun, "Olivine LiFePO4: The remaining challenges for future energy storage," *Energy Environ. Sci.*, vol. 8, no. 4, pp. 1110–1138, 2015, doi: 10.1039/c4ee04016c.

[25] F. Renard, "2020 cathode materials cost competition for large scale applications and promising LFP best-in-class performer in term of price per kWh," *Int. Conf. Olivines Recharg. Batter.*, 2014, [Online]. Available: https://www.eiseverywhere.com/file_uploads/eb9b04cd75ee9da4619308dfffd78760_O-8.01RenardFabrice.pdf.

[26] K. Zaghib *et al.*, "Review and analysis of nanostructured olivine-based lithium recheargeable batteries: Status and trends," *J. Power Sources*, vol. 232, pp. 357–369, 2013, doi: 10.1016/j.jpowsour.2012.12.095.

[27] P. Albertus, S. Babinec, S. Litzelman, and A. Newman, "Status and challenges in enabling the lithium metal electrode for high-energy and low-cost rechargeable batteries," *Nat. Energy*, vol. 3, no. 1, pp. 16–21, 2018, doi: 10.1038/s41560-017-0047-2.

[28] W. Xu *et al.*, "Lithium metal anodes for rechargeable batteries," *Energy Environ. Sci.*, vol. 7, no. 2, pp. 513–537, 2014, doi: 10.1039/c3ee40795k.

[29] O. Crowther and A. C. West, "Effect of Electrolyte Composition on Lithium Dendrite Growth," *J. Electrochem. Soc.*, vol. 155, no. 11, p. A806, 2008, doi: 10.1149/1.2969424.

[30] M. N. Obrovac and V. L. Chevrier, "Alloy negative electrodes for Li-ion batteries," *Chem. Rev.*, vol. 114, no. 23, pp. 11444–11502, 2014, doi: 10.1021/cr500207g.

[31] Y. P. Wu, E. Rahm, and R. Holze, "Carbon anode materials for lithium ion batteries," *J. Power Sources*, vol. 114, no. 2, pp. 228–236, 2003, doi: 10.1016/S0378-7753(02)00596-7.

[32] X. Sun, P. V. Radovanovic, and B. Cui, "Advances in spinel Li4Ti5O12 anode materials for lithium-ion batteries," *New J. Chem.*, vol. 39, no. 1, pp. 38–63, 2015, doi: 10.1039/c4nj01390e.

[33] Z. Chen, I. Belharouak, Y. K. Sun, and K. Amine, "Titanium-based anode materials for safe lithium-ion batteries," *Adv. Funct. Mater.*, vol. 23, no. 8, pp. 959–969, 2013, doi: 10.1002/adfm.201200698.

[34] R. Korthauer, *Lithium-ion batteries: Basics and applications*. 2018.

[35] G. G. Eshetu *et al.*, "Fire behavior of carbonates-based electrolytes used in Li-ion rechargeable batteries with a focus on the role of the LiPF6 and LiFSI salts," *J. Power Sources*, vol. 269, pp. 804–811, 2014, doi: 10.1016/j.jpowsour.2014.07.065.

[36] K. Xu, "Nonaqueous liquid electrolytes for lithium-based rechargeable batteries," *Chem. Rev.*, vol. 104, no. 10, pp. 4303–4417, 2004, doi: 10.1021/cr030203g.

[37] H. Yang, G. V. Zhuang, and P. N. Ross, "Thermal stability of LiPF6 salt and Li-ion battery electrolytes containing LiPF6," *J. Power Sources*, vol. 161, no. 1, pp. 573–579, 2006, doi: 10.1016/j.jpowsour.2006.03.058.

[38] J. Kalhoff, D. Bresser, M. Bolloli, F. Alloin, J. Y. Sanchez, and S. Passerini, "Enabling LiTFSI-based electrolytes for safer lithium-ion batteries by Using linear fluorinated carbonates as (Co)solvent," *ChemSusChem*, vol. 7, no. 10, pp. 2939–2946, 2014, doi: 10.1002/cssc.201402502.

[39] V. Aravindan, J. Gnanaraj, S. Madhavi, and H. K. Liu, "Lithium-ion conducting electrolyte salts for lithium batteries," *Chem. - A Eur. J.*, vol. 17, no. 51, pp. 14326–14346, 2011, doi: 10.1002/chem.201101486.

[40] M. Dahbi, F. Ghamouss, F. Tran-Van, D. Lemordant, and M. Anouti, "Comparative study of EC/DMC LiTFSI and LiPF6 electrolytes for electrochemical storage," *J. Power Sources*, vol. 196, no. 22, pp. 9743–9750, 2011, doi: 10.1016/j.jpowsour.2011.07.071.

[41] Y. Hu, H. Li, X. Huang, and L. Chen, "Novel room temperature molten salt electrolyte based on LiTFSI and acetamide for lithium batteries," *Electrochem. commun.*, vol. 6, no. 1, pp. 28–32, 2004, doi: 10.1016/j.elecom.2003.10.009.

[42] K. Xu, S. S. Zhang, U. Lee, J. L. Allen, and T. R. Jow, "LiBOB: Is it an alternative salt for lithium ion chemistry?," *J. Power Sources*, vol. 146, no. 1–2, pp. 79–85, 2005, doi: 10.1016/j.jpowsour.2005.03.153.

[43] K. Xu, S. Zhang, T. R. Jow, W. Xu, and C. A. Angell, "LiBOB as salt for lithium-ion batteries. A possible solution for high temperature operation," *Electrochem. Solid-State Lett.*, vol. 5, no. 1, 2002, doi: 10.1149/1.1426042.

[44] B. Scrosati and C. A. Vincent, "Polymer electrolytes: The key to lithium polymer batteries," *MRS Bull.*, vol. 25, no. 3, pp. 28–30, 2000, doi: 10.1557/mrs2000.15.

[45] R. G. Regulation and B. Y. Auxin, "Further 1986. 37:407-38," 1986.

[46] A. Manuel Stephan and K. S. Nahm, “Review on composite polymer electrolytes for lithium batteries,” *Polymer (Guildf).*, vol. 47, no. 16, pp. 5952–5964, 2006, doi: 10.1016/j.polymer.2006.05.069.

[47] P. G. Bruce, “Structure and electrochemistry of polymer electrolytes,” *Electrochim. Acta*, vol. 40, no. 13–14, pp. 2077–2085, 1995, doi: 10.1016/0013-4686(95)00144-4.

[48] A. Bouridah, F. Dalard, D. Deroo, and M. B. Armand, “Potentiometric measurements of ionic transport parameters in poly(ethylene oxide)-LiX electrolytes,” *J. Appl. Electrochem.*, vol. 17, no. 3, pp. 625–634, 1987, doi: 10.1007/BF01084138.

[49] W. Huang *et al.*, “Quasi-solid-state rechargeable lithium-ion batteries with a calix[4]quinone cathode and gel polymer electrolyte,” *Angew. Chemie - Int. Ed.*, vol. 52, no. 35, pp. 9162–9166, 2013, doi: 10.1002/anie.201302586.

[50] T. T. Zuo *et al.*, “Constructing a Stable Lithium Metal-Gel Electrolyte Interface for Quasi-Solid-State Lithium Batteries,” *ACS Appl. Mater. Interfaces*, vol. 10, no. 36, pp. 30065–30070, 2018, doi: 10.1021/acsami.8b12986.

[51] S. Tang, W. Guo, and Y. Fu, “Advances in Composite Polymer Electrolytes for Lithium Batteries and Beyond,” *Adv. Energy Mater.*, vol. 2000802, pp. 1–29, 2020, doi: 10.1002/aenm.202000802.

[52] Y. Jiang *et al.*, “Development of the PEO based solid polymer electrolytes for all-solid state lithium ion batteries,” *Polymers (Basel).*, vol. 10, no. 11, pp. 1–13, 2018, doi: 10.3390/polym10111237.

[53] W. Li, Y. Pang, J. Liu, G. Liu, Y. Wang, and Y. Xia, “A PEO-based gel polymer electrolyte for lithium ion batteries,” *RSC Adv.*, vol. 7, no. 38, pp. 23494–23501, 2017, doi: 10.1039/c7ra02603j.

[54] M. M. E. Jacob, S. R. S. Prabaharan, and S. Radhakrishna, “Effect of PEO addition on the electrolytic and thermal properties of PVDF-LiClO4 polymer electrolytes,” *Solid State Ionics*, vol. 104, no. 3–4, pp. 267–276, 1997, doi: 10.1016/s0167-2738(97)00422-0.

CHAPTER 2. EXPERIMENTAL METHODS AND THEORY

2.1 Chemical and Materials

PEO (Sigma Aldrich, M_w = 600,000 g mol^{-1}), PEGDA (Sigma Aldrich, 99%, MW = 700 g mol^{-1}), PC (Alfa Aesar, 99%), DEC (Sigma Aldrich, 99%), photoinitiator phenylbis(2,4,6-trimethylbenzoyl)phosphine oxide (Irgacure 819®, Sigma Aldrich, 97%), LiBOB (Sigma Aldrich), LiTFSI (Sigma Aldrich), NMP (Fisher Scientific, 99%), polypropylene separator (2400, Celgard) and PVDF (Sigma Aldrich, Mw ~ 534,000 g mol^{-1}) were purchased. Conductive carbon black (Super P), LFP powder, LTO powder and CR2032 coin-cell fabrication components (cases, spacer, spring) were purchased from MTI corporation. All the chemicals were used without any additional purification or treatment.

2.2 Equipment for Measurements

2.2.1 Morphology and Structural Analysis

Scanning electron microscopy (SEM, Vega3, TESCAN) was used to investigate the morphology of the LFP and LTO electrode. Thermogravimetric analysis (TGA, TG 209 F1 Libra, Netzsch) and differential scanning calorimetry (DSC, Polyma, Netzsch) were operated to measure the thermal stability of GPEs, and changes of energy absorbed or release to determine the crystalline transition temperature and melting temperature. The crystallinity of GPEs was measured by X-ray diffraction (XRD, Empyrean Series 2, PANalytical).

2.2.2 Electrochemical Analysis

LSV, CV and AC impedance spectra were carried out with a potentiostat/galvanostat (VersaSTAT 4, AMETEK) to determine the oxidative stability window of GPEs, redox reaction of electrodes as potential changes, and electrochemical impedance of GPEs, respectively. Electrochemical charge/discharge profiled, and cycling performance were implemented by a battery test system (BT2000, ARBIN) with CR2032 coin-cells composed of LFP and LTO for cathode and anode, respectively.

2.3 Cell Preparation

2.3.1 Electrode Preparation

For the cathode preparation, LFP powder, carbon black, and PVDF were measured and mixed in 8:1:1 weight ratio. The powders were placed in a glass vial and NMP solvent was added to the mixture followed by a vigorous stirring at RT overnight. The slurry was then casted on an Al foil by doctor blading with 120 μm spacer to form the cathode layer and then dried at 120 ℃ on a hotplate overnight to remove the solvents. For the anode side, the mixture was prepared with LTO powder instead of LFP powder with the same weight ratio. The LTO slurry coating followed the same procedure but coated on a Cu foil instead of Al foil. Figure 2.1 shows the LFP and LTO coating on the current collector. Figure 2.2 shows the surface morphology of the LFP and LTO coating.

Figure 2. 1 Electrode preparation for LFP casted on the Al foil (left) and LTO casted on the Cu foil (right)

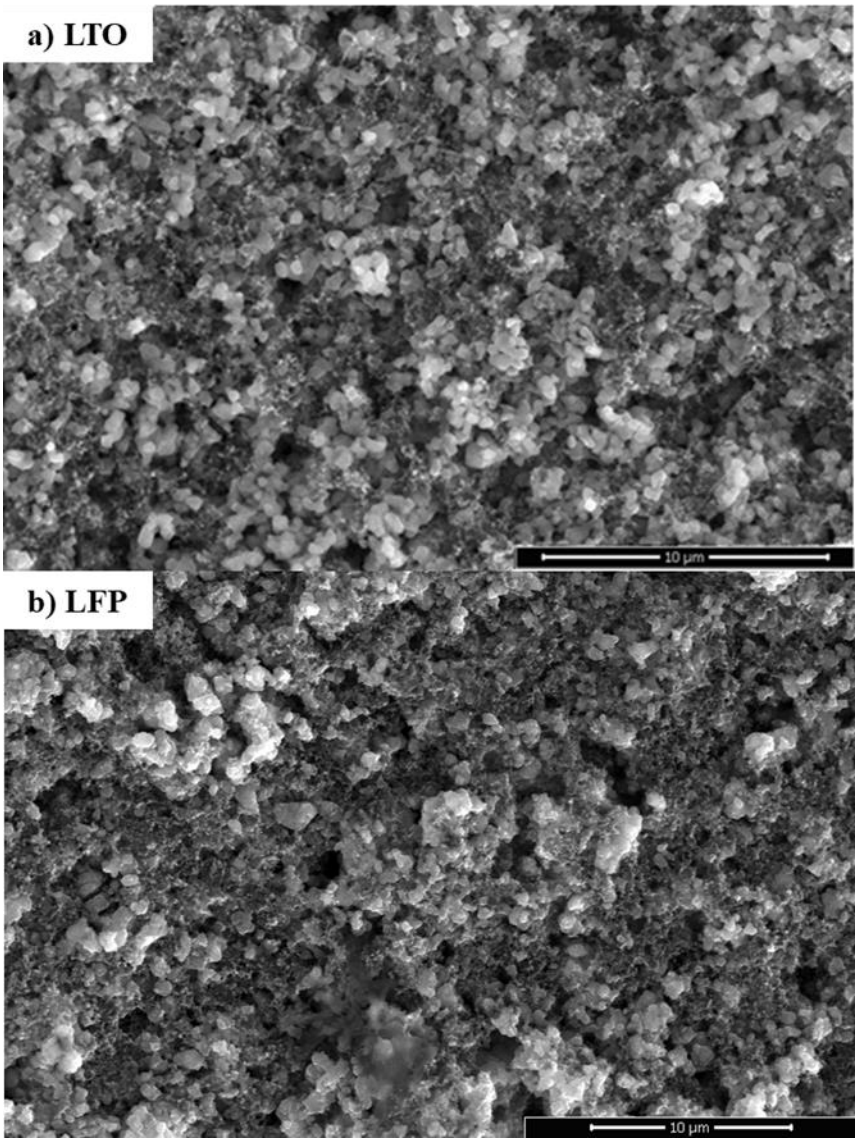

Figure 2. 2 SEM images of a) LFP surface and b) LTO surface

2.3.2 Electrolyte Preparation

2.3.2.1 Liquid Electrolytes

For the comparison, a LiBOB-based liquid electrolyte was prepared due to its high ionic conductivity of 8.2 x 10^{-3} S/cm. [1] 0.6 m LiBOB was completely dissolved in PC and DEC solvent (1:1 weight ratio). The mixture was further stirred at RT to prepare a colorless electrolyte solution.

2.3.2.2 Gel Polymer Electrolytes

The 0.7 g mixture of prepolymer host PEGDA and PC with 6 different ratios (6:1, 5:2, 4:3, 3:4, 2:5, and 1:6) were added to 0.3 g LiTFSI, keeping the total weight of mixture 1g. LiBOB salt at 2 wt% in respect to the whole mixture was added and stirred for 1 hr allowing the salt to be completely dissolved. Irgacure 819 photoinitiator at 2 wt% in respect to the PEGDA was then added to the LiBOB solution, and the mixture was further stirred for another 1 hr. Figure 2.3 shows the process preparing the GPEs. The yellowish mixture was left to rest for 10 min in order to allow the bubbles to defoam. Subsequently, the mixture was poured into a glass mold with a diameter of 15mm, and desired depth of thickness (250 μm). A UV light source with a wavelength of 350 nm (Solar simulator, 450 W) was exposed to the sample for 1 min to obtain a solvent-free, free-standing GPE film with a diameter of 14 mm. The UV light intensity was measured as 0.02 mW/cm^2.

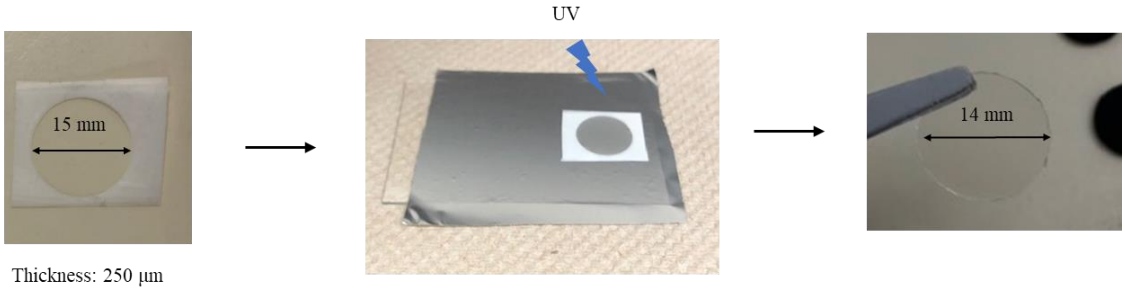

Figure 2. 3 A preparation procedure for the GPEs

2.3.2.3 PEO-based gel polymer electrolytes

PEO-based gel polymer electrolytes were prepared by mixing PEO, PC, LiTFSI and LiBOB. To investigate the effect of plasticizer and lithium salts, total 3 sets of samples were prepared. Firstly, the effect of LiBOB salt was studied by varying its concentration. 1.0 M LiTFSI was added to 0.1 g of PEO followed by adding LiBOB salt as an additive with the amount of 0.02 g, 0.05 g, 0.1 g, and 0.2 g, respectively, to form gel polymer matrix. Then, the amount of PC was increased from 0.1 ml to 0.2 ml for 0.5 M LiTFSI and 0.5 M LiBOB solutions while the amount of PEO was fixed at 0.1 g. When the 0.5 M LiTFSI was introduced to the PEO, 0.02 g, 0.05 g, 0.1 g, and 0.2 g of LiBOB was added to the mixture. By contrast, when the 0.5 M LiBOB was applied to the PEO, LiTFSI was used as an additive with the amount of 0.02 g, 0.05 g, 0.1 g, and 0.2 g. After the mixture was placed in a vial, the vial was heated on a hotplate to 70 ℃ for 24 hr. The slurry was further stirred by a stirring rod vigorously to complete mixing. As shown in Figure 2.4, the PEO-based slurry exhibits a sticky gel chunk that is flexible.

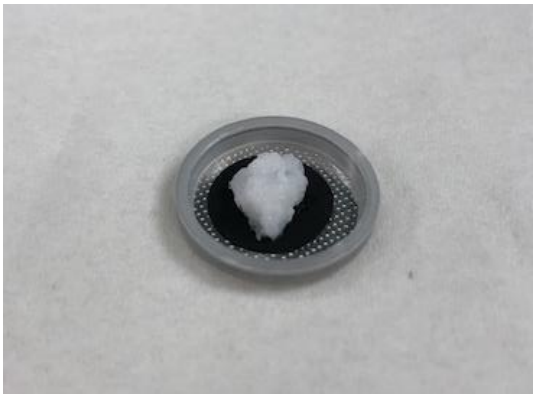

Figure 2. 4 PEO-based GPE electrolyte on the LFP electrode and CR2032 case

2.3.3 Cell assembly

The prepared LFP and LTO electrodes were punched into 12.5 mm diameter circular discs for cathode and anode for coin-cell battery, respectively, and then soaked with the 0.6 m LiBOB liquid electrolyte or liquid precursor of GPEs followed by placing a separator for the liquid electrolyte, the GPE film, or the PEO-based GPE on the top of the soaked electrode. The CR2032 coin-cell was assembled as shown in Figure 2.5. The cathode electrode was placed on the positive case followed by the liquid or GPE electrolytes. For the liquid electrolyte use, a separator was placed between the electrodes and the spacer and spring were placed onto the anode. When the GPE was used, the separator was not used since the GPE could separate properly the electrodes playing a role as a separator. The rest part of the assembly is same as the liquid used coin-cell. The completed configuration of liquid and GPE electrolyte coin cell batteries are LFP/liquid electrolyte/LTO and LFP/GPE/LTO, respectively.

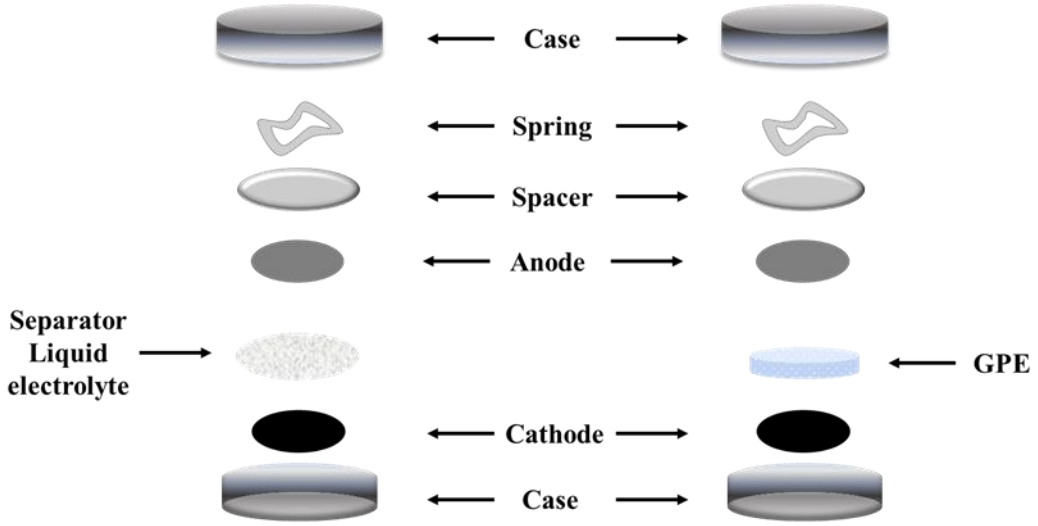

Figure 2. 5 Schematic image of CR2032 coin-cell assembly for liquid electrolyte (left) and GPE electrolytes (right)

2.4 Fundamental Background Theory

2.4.1 Thermogravimetric Analysis (TGA)

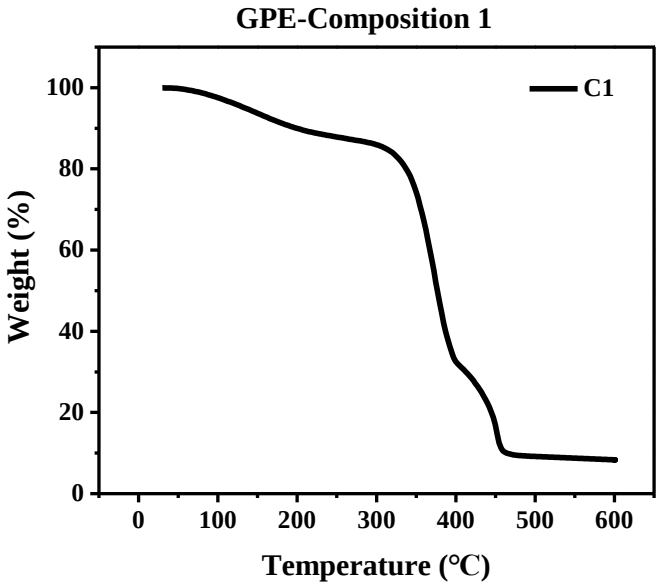

Figure 2. 6 TGA curve for GPE-C1(60/10/30)

TGA is an important technique used for the thermal characterization of material through measuring the change of mass as the change of temperature in a desired atmosphere. With the loss of weight as temperature increases, it can be determined for the types and content of volatile materials in the sample as well as the decomposition temperature of compound. On the other hand, the weight increase with the elevating temperature indicates the oxidation of the sample under an oxidizing atmosphere. Nitrogen or argon gases are mainly used for generating inert atmosphere and for oxidizing atmosphere, air or oxygen environment be used. An example for TGA curve is represented in Figure 2.6. Where step 1 from 100 ℃ to 300 ℃ indicates the evaporation of water content, and step 2 from 300 ℃ to 400 ℃ represents the decomposition. [2]

2.4.2 Differential Scanning Calorimetry (DSC)

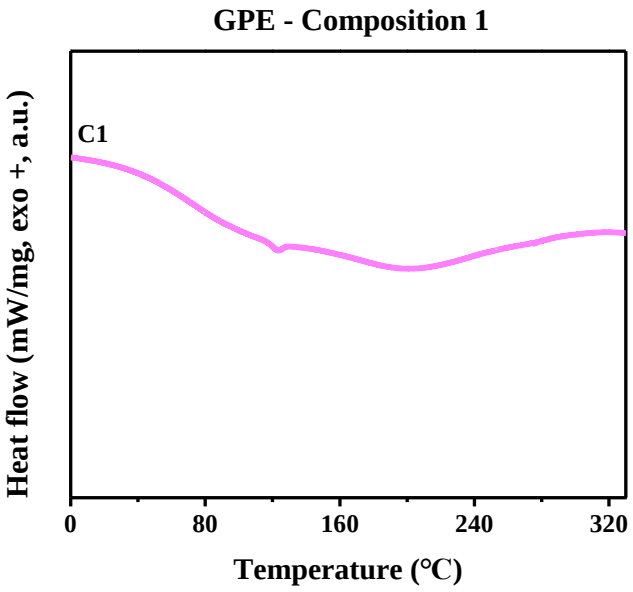

Figure 2. 7 DSC curve for GPE-C1(60/10/30)

DSC can determine the melting temperature, heat of fusion, latent heat of melting, reaction energy and temperature, glass transition temperature, crystalline phase transition temperature and energy, precipitation energy and temperature, denaturization temperatures, oxidation induction times, and specific heat capacity by detecting the energy transfer of a sample by measuring a physical or chemical change. Also, DSC analysis measures the amount of energy absorbed or released by a sample when the sample is heated or cooled, and it provides with quantitative and qualitative data on endothermic (heat absorption) and exothermic (heat evolution) processes. In this dissertation, DSC is specifically used to investigate the change of crystalline phase transition temperature of the GPE by adding the organic solvent, as show in Figure 2.7. [3]

2.4.3 X-ray diffraction (XRD) Analysis

XRD analysis is a powerful nondestructive technique for characterizing physical structure of crystalline materials. The XRD measurement provides with information on, phases, and other structural parameters, such as average grain size, crystallinity, strain, and crystal defects. The XRD peak appears when detecting the crystallinity and its intensities are determined by the atomic positions within the lattice planes. Thus, the XRD pattern can be the fingerprint of periodic atomic arrangements in the sample materials. Herein, with the DSC analysis, XRD is used to study the impact of plasticizer to GPE by focusing the crystallinity change of GPE. [4]

2.5 Electrochemical Characterization

2.5.1 Cyclic Voltammetry (CV)

CV is one of the most common electrochemical technique measuring the current response against scanned potential at the interface of working electrode and electrolyte in order to understand the redox reaction mechanisms or to perform quantitative analysis. A typical cyclic voltammogram is represented in Figure 2.8. The cyclic voltammogram of Figure 2.8 is an example of single-electron transfer redox reaction and it can be represented as

$$M^+ + e^- \rightleftharpoons M$$

The potential change from (a) the initial to (d) the switching indicates a reduction caused by the negative scanning, which is called cathodic current (i_{pc}). The peak potential at (c) represents the cathodic peak potential (E_{pc}) where all of the substrate at the surface of the

electrode has been reduced. After that, the positive potential scans take place from (d) to (g), and the oxidation occurs in anodic current (I_{pa}). The anode peak potential (E_{pa}) is defined at the peak potential (f) where all of the substrate at the surface of the electrode has been oxidized.

For reversible systems, the formal reduction potential ($E°'$) can be determined by following equations:

$$E = E_i + vt$$

where, E_i is the initial potential in volts, v is the sweep rate in volts/s, and t is the time in seconds. When the direction switched, the equation turns to

$$E = E_s - vt$$

where, E_s is the potential at the switching point. Electron stoichiometry (n):

$$E_p - E_{\frac{p}{2}} > \frac{0.0565}{n}$$

where, E_{pa} is the anodic peak potential, E_{pc} is the cathodic peak potential, and n is the number of electrons participating in the redox reactions. Thus, formal reduction is calculated as the mean of the E_{pa} and E_{pc} values: [5]

$$E°' = \frac{E_{pa} + E_{pc}}{2}$$

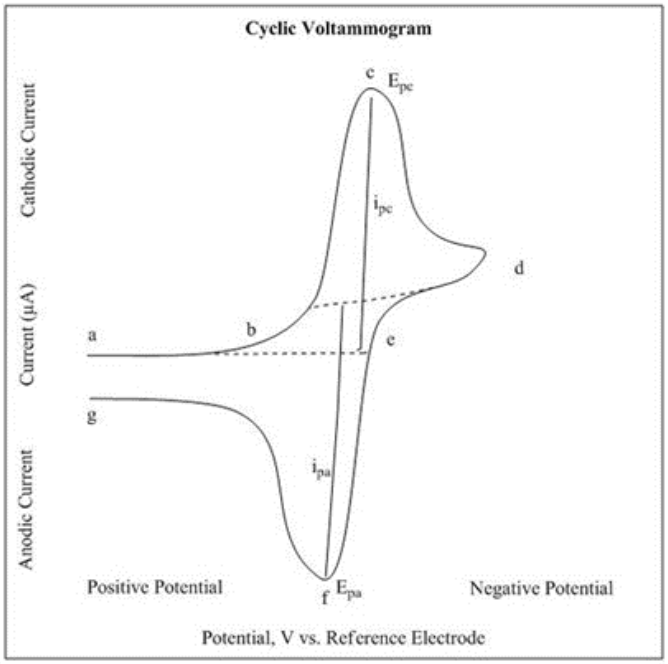

Figure 2. 8 Cyclic voltammogram [5]

2.5.2 Linear Sweep Voltammetry (LSV)

LSV, well-established technique as a fast and reliable characterization, is a basic voltammetric method that measures the current at a working electrode as a function of voltage per time, scan rate (V/s) by linearly sweeping the potential between the working electrode and a reference electrode. A common output of LSV measurements represents the current vs potential as shown in Figure 2.9. Also, when the oxidation or reduction of species begins at the potential, a peak in the current signal can be monitored. Thus, both qualitative and quantitative information about the redox process through the electrochemical system can be determined by utilizing LSV technique. [5]

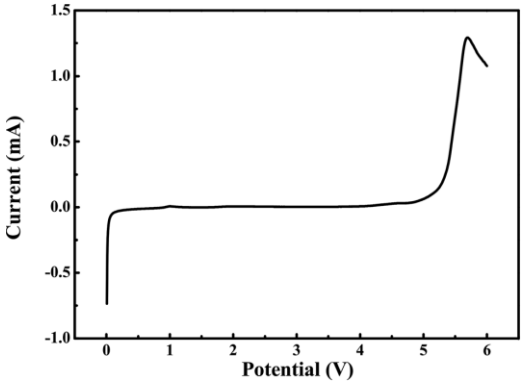

Figure 2. 9 LSV of the PEO-based gel polymer electrolyte at 0.5 mV/s [6]

2.5.3 Electrochemical Impedance Spectroscopy (EIS)

EIS is an electrochemical technique to determine the electrochemical response as a function of frequency such as internal and interfacial impedance, by measuring the impedance of a system when an AC potential is applied to the system. Nyquist plot is generally used to display the impedance trace on the complex plane. The Nyquist plot is composed of a real and an imaginary part for the X-axis and Y-axis, respectively, and can be plotted from a following equation where the impedance is represented as a complex number,

$$Z_\omega = \frac{E_\omega}{I_\omega} = Z_0 \exp(j\varphi) = Z_0(\cos\varphi + jsin\varphi)$$

where, E_ω = frequency-dependent potential, I_ω = frequency-dependent current. The Y-axis represents negative and each point on the plot is the impedance at one frequency.

An impedance caused by diffusion can be created, which is called a Warburg impedance. Warburg impedance represents small at high frequencies because the reactants do not diffuse far, while the impedance is increasing at low frequencies since the reactants diffuse

farther. The Warburg impedance appears as a diagonal line with a slope of 45º in the Nyquist plot. [7]

When polarization occurs due to combination of kinetic and diffusion process, the one semi-circle is not sufficient. In this case, a Warburg diffusion is added to the semi-circle and it is plotted as shown in Figure 2.10.

For the electrochemical system of LIBs, it is commonly observed that there are two semi-circles with a Warburg impedance as shown in Figure 2.11. The first semi-circle at high-frequency represents the interfacial resistance between the electrolyte and the symmetric electrode. Meanwhile the second semi-circle at the medium frequency is a result from the charge transfer resistance between the electrode and the conductive agent of electrolyte. The semi-infinite Warburg line is contributed to the diffusion. [7, 8]

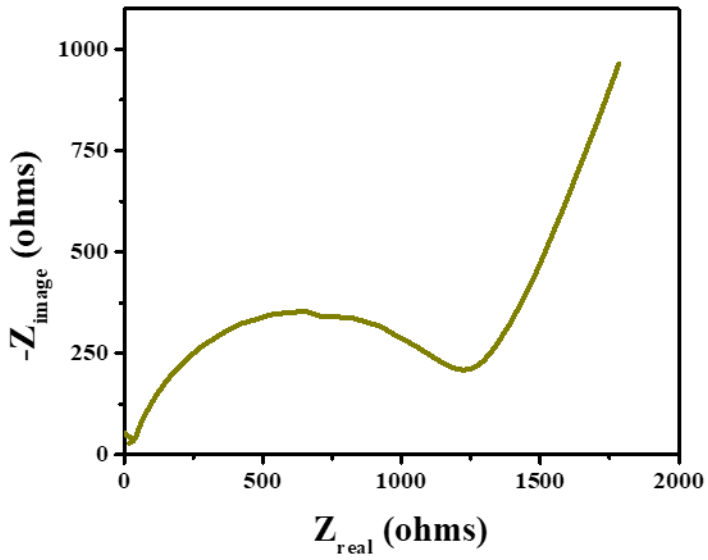

Figure 2. 10 Nyquist plot for mixed kinetic and diffusion system

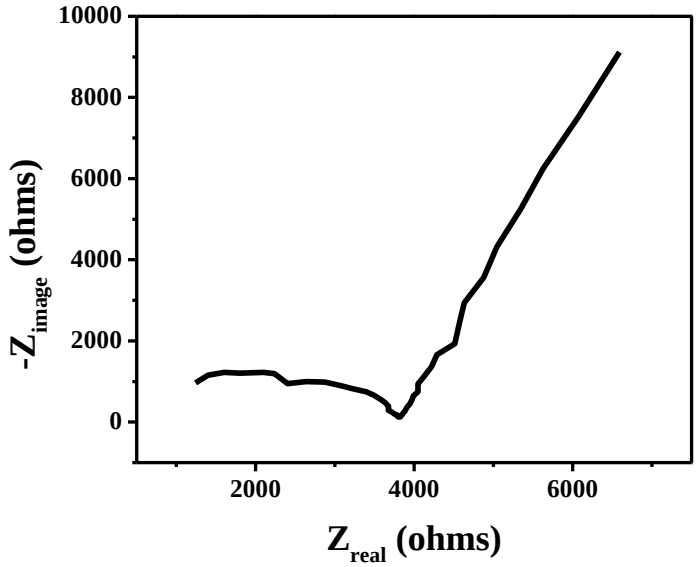

Figure 2. 11 Typical Nyquist plot with two semi-circles and a Warburg

2.5.4 Ionic Conductivity

The ionic conductivity is a measure of electrolytes' tendency to ionic conduction between the electrodes through the electrolyte. Generally, the ionic conductivity is measured by the EIS with a cell which the electrolyte film is placed in between two stainless steel electrodes. Then, the ionic conductivity was calculated by the following formula;

$$\sigma = \frac{l}{R_b A}$$

where, l and A are the thickness and area of the electrolyte film R_b is the bulk resistance of the electrolyte film, which is determined from the X-axis of Nyquist plot. [9]

2.5.5 Battery Performance

To determine the charge and discharge capacity (mAh/g), the galvanostatic charge and discharge tests are performed for the CR2032 coin-cell. A constant current of 0.1 C is applied to the charging and discharging process. A cut-off voltage is set-up by defining the limit value based on the CV test. Also, the cyclic stability of a battery is evaluated at a constant current of 0.1 C. For the coin-cell constitution, LFP/liquid electrolyte/LTO or LFP/GPE/LTO cell was used for the charge/discharge profiles and cycling performance at 0.1 C with a voltage cut-off ranging of 1.2 – 2.4 V.

Reference

[1] M. S. Ding, K. Xu, and T. R. Jow, "Conductivity and Viscosity of PC-DEC and PC-EC Solutions of LiBOB," *J. Electrochem. Soc.*, vol. 152, no. 1, p. A132, 2005, doi: 10.1149/1.1833611.

[2] R. Bottom, "Thermogravimetric Analysis," *Princ. Appl. Therm. Anal.*, vol. 1, no. 906, pp. 87–118, 2008, doi: 10.1002/9780470697702.ch3.

[3] F. Q. Samples, T. U. S. Standard, and S. Series, "Dean's analytical chemistry handbook," *Choice Rev. Online*, vol. 42, no. 03, pp. 42-1566-42–1566, 2004, doi: 10.5860/choice.42-1566.

[4] R. G. Teller, "Modern powder diffraction," *J. Solid State Chem.*, vol. 86, no. 2, p. 340, 1990, doi: 10.1016/0022-4596(90)90153-o.

[5] P. T. Kissinger and W. R. Heineman, "Cyclic voltammetry," *J. Chem. Educ.*, vol. 60, no. 9, pp. 702–706, 1983, doi: 10.1021/ed060p702.

[6] W. Li, Y. Pang, J. Liu, G. Liu, Y. Wang, and Y. Xia, "A PEO-based gel polymer electrolyte for lithium ion batteries," *RSC Adv.*, vol. 7, no. 38, pp. 23494–23501, 2017, doi: 10.1039/c7ra02603j.

[7] R. Cao, Q. C. Zhuang, L. L. Tian, X. Y. Qiu, and Y. L. Shi, "Electrochemical impedance spectroscopic study of the lithium storage mechanism in commercial molybdenum disulfide," *Ionics (Kiel).*, vol. 20, no. 4, pp. 459–469, 2014, doi: 10.1007/s11581-013-0996-9.

[8] S. A. Mohd Noor, D. Gunzelmann, J. Sun, D. R. MacFarlane, and M. Forsyth, "Ion conduction and phase morphology in sulfonate copolymer ionomers based on ionic liquid-sodium cation mixtures," *J. Mater. Chem. A*, vol. 2, no. 2, pp. 365–374, 2014, doi: 10.1039/c3ta13835f.

[9] M. Safa, A. Chamaani, N. Chawla, and B. El-Zahab, "Polymeric Ionic Liquid Gel Electrolyte for Room Temperature Lithium Battery Applications," *Electrochim. Acta*, vol. 213, pp. 587–593, 2016, doi: 10.1016/j.electacta.2016.07.118.

CHAPTER 3. DEVELOPMENT OF A GEL POLYMER ELECTROLYTE FOR A SAFE FULL CELL

3.1 Introduction

The tremendous efforts have been devoted to develop a sustainable energy supply to reduce a dependence on the fossil fuels and the field of energy storage has become one of the most important areas of research. [1, 2] Among the energy storage systems, LIBs have succeeded as the most widely commercialized energy storage for the consumer electronic market. [3-5]

However, the fire safety of LIBs has been one of the serious hazards threatening the use of LIBs as the commercial applications such as portable, electronic vehicles (EVs), and stationary energy storage system. [6, 7] The safety issue of LIBs generally is caused by both from the instability and flammability of the liquid organic electrolytes and the electrode materials. [6, 8 ,9] Replacing the liquid organic electrolytes with solid-state electrolytes composed of polymers or inorganic materials has been considered one of the effective ways to improve the safety of electrolytes. [10] Specifically, GPEs have overcome the major drawback of solid-polymer electrolytes such as low ionic conductivity at RT since they possess both solid and liquid properties such as mechanical strength and high ionic conductivity. [11–13] Although it still has been under a debate that the crystalline of polymer electrolytes can offer the higher conductivity than the amorphous of that, [14, 15] it has been generally admitted that the lithium ions transported in the amorphous regions but the crystalline regions of the polymer electrolytes hindered the

migration of ions. [16–18] There are many techniques have been developed to enhance the ionic conductivity by increasing the amorphous phase of polymers, and plasticization is one of the handy and cost-effective way. [19] Organic liquid plasticizers such as EC, PC, and DMC can be mixed with polymer hosts due to their high dielectric constant and low viscosity as shown in Table 1.1, and it results in the formation of gel-like electrolytes. [20] However, although increasing the amorphousness of the GPE increase the ionic conductivity, the GPE can be suffered by low cation transport number (Li^+), which could cause the deterioration of electrodes. [21] Lithium salts with large anions could be introduced to the GPE to improve the transport number while increasing the amorphous phase of the polymer electrolytes. [22] The LiTFSI has been considered as one of the best salts for PEO-based polymer electrolytes owing to their high charge delocalization of ionic dissociation in the PEO polymer as well as decreasing the crystallinity of polymer. [23] However, it is reported that LiTFSI react with the aluminum current collector, causing the severe corrosive effect resulting in limited cycle performance and low coulombic efficiency. [24] In order to prevent the corrosive effects of LiTFSI, LiBOB can be added to the LiTFSI electrolyte as an additive since the LiBOB passivates the aluminum current collector. [25]

Another effective way to develop the safe LIBs is to replace the conventional electrodes with chemically more stable materials. For cathode materials, $LiCoO_2$ cathode used in conventional LIBs has reported that oxygen release caused by an unexpected operating condition such as overcharge that exceeds the oxidative limit of electrolyte, can react with the flammable organic liquid, which lead to the safety hazard. [6, 26] Alternatively,

$LiMn_2O_4$ has been considered for a while due to their good thermal stability, however, it has been recognized that manganese dissolves in the liquid electrolyte on cycling in lithium cells at temperatures above ambient. [27] Thus, herein, LFP for a cathode material operating at 3.5V (vs. Li/Li^+) with a theoretical capacity of 170 mAh/g is selected to achieve the safe LIBs due to its stability, excellent cycling stability, relatively low-cost and environmental friendliness. [27, 28] It is recognized that LFP is chemically more stable that $LiCoO_2$ because PO_4 group of LFP has stronger covalent bonds than that of CoO_2 group of $LiCoO_2$. [6]

Similarly, titanium-based anode material, LTO, is here used as a substitute for the conventional anode material, graphite, to improve the safety perspective. LTO possesses the long cycle life, excellent safety characteristics and lithium-ion insertion and extraction reversibility, negligible volume change during the charge-discharge process, and a flat potential plateau. [29]. It has been considered to replace the conventional graphite anode material due to its thermal instability of a SEI layer. For instance, at elevated temperature (> 60 ℃), the SEI on the graphite surface formed during the initial charging and discharging at 0.8 V (vs. Li/Li^+) tends to decompose and formation repeatedly leading to a continuous heat flow and eventually trigger the thermal runway. [30] Meanwhile, the use of LTO for anode material is advantageous that the formation of an SEI film can be avoided because it operates at higher potential of ~ 1.55 V (vs. Li/Li^+), delivering a theoretical capacity of (175 mAh/g). [31, 32] In a full-cell configuration, it is important to match the capacity balance between the cathode and anode. Mostly, the capacity of anode is not less than that of cathode otherwise the lithium plating occurs when the cell is fully charged. [32]

Also, the Li-ion from the lithiated cathode material is the only source to utilize unlike the half-cell where Li metal acts as a reservoir for Li-ions. [33] Thus, it is not ideal to consume the Li-ions for the side reaction during continuous electrochemical processes, directly contribute to the capacity loss of the cell. [32] In this respect of compatible specific capacity and high operating potential to avoid the side reaction, the combination of LFP and LTO for cathode and anode, respectively, can be a suitable candidate, especially, for the stationary applications. This is because stationary applications desire are low-cost, long cycle life, long calendar life span, and safety over energy and power. [29, 34]

Herein, a full-cell with gel polymer electrolytes that enables to be assembled in ambient conditions is reported, which is composed of LFP as a cathode, LTO as an anode, and GPEs with different compositions. The GPEs was prepared from LiTFSI and LiBOB as lithium salt and additive respectively, PC as plasticizer and PEGDA prepolymer hosts. The low molecular weight of PEGDA allowed complete mixing with salt and plasticizer. Through a crosslinking reaction, a free-standing, holding the formation without a support material, GPE film was achieved. Electrochemical and thermal characterizations were carried out to determine the stability the stability of the GPEs. Electrochemical performance evaluation of LIBs of LFP/GPE/LTO demonstrated that the novel polymer electrolyte exhibited excellent electrochemical stability during long cycle testing.

3.2 Experimental

3.2.1 Gel Polymer Electrolyte Preparation

The detailed experimental procedures are described in Chapter 2. As Table 3.1 shows, the GPEs were prepared in six different composition in weight ratio between PEGDA, PC, and LiTFSI followed by 2 wt% of LiBOB as an additive (in respect to the whole mixture). From C1 to C6, the amount of PEGDA decreased from 60 wt% to 10 wt% at 10 wt% interval while the amount of PC increased from 10 wt% to 60 wt% at 10 wt% interval with the fixed amount of 2 wt% LiBOB for each composition, and the total weight was kept to 1 g. The photoinitiator (Irgacure 819®) at 2 wt% in respect to the PEGDA was then added to the transparent mixture to trigger the UV-crosslinking for GPEs. A UV light source with a wavelength of 350 nm (Solar simulator, 450 W) was exposed to the sample for 1 min to obtain the GPE film. The UV light intensity was measured as 0.02 mW/cm^2.

For a comparison with GPE electrolytes, a 0.6 m LiBOB dissolved in PC-DEC (1:1 weight ratio) liquid electrolyte was prepared. The process for GPEs and liquid electrolyte was carried out in the ambient-conditions, without the inert atmosphere.

Table 3. 1 Different composition for GPEs

Composition	PEGDA (wt%)	PC (wt%)	LiTFSI (wt%)	LiBOB (wt%)
1	60	10	30	2
2	50	20	30	2
3	40	30	30	2
4	30	40	30	2
5	20	50	30	2
6	10	60	30	2

3.2.2 Thermal Analysis of GPE

Glass transition temperature (T_g), melting temperature (T_m) and crystallinity of the GPE film was determined by the utilization of the DSC (DSC 214 Polyma, Netzsch), where the temperature range was scanned from -40 to 350 ℃ at a temperature ramping rate of 10 ℃/min. The GPE film samples for the DSC were pre-dried overnight in the fume hood. The TGA (TG 209 F1 Libra, Netzsch) was used to determine the weight percentage component of the thermal stability of the GPE. The temperature was measured from 30 to 600 ℃ at a rate of 10 ℃/min under nitrogen atmosphere for the weight percentages of different components.

3.2.3 SEM, XRD and FT-IR Characterization

The structural characterization of the GPE was characterized by the XRD (Empyrean Series2, PANalytical) with Cu Kα radiation (λ = 1.5406Å) at an accelerating voltage set at 40 kV with 40 mA in the 2θ range of 5-50º, and by the FT-IR (Nicolet iS10, Thermo Scientific), using scan number of 16 and resolution of 4. The morphology image of the electrodes was characterized by the SEM (Vega3, TESCAN) operating at 20 kV.

3.2.4 Electrodes Preparation and Full-cell Fabrication

The detailed experimental procedure is described in Chapter 2. The LFP cathode and LTO anode, respectively, were prepared followed by 80:10:10 weight ratio between active material (LFP or LTO), carbon black, and polymer binder (PVDF). As shown in Figure

2.5, CR2032 coin-cell was used to assemble LFP/liquid electrolyte/LTO and LFP/GPE/LTO batteries. For the liquid electrolyte (0.6 m LiBOB), a separator was placed between the cathode and anode electrodes to separate them to prevent the internal shortage. When the coin-cell for GPEs was assembled, a separator was not required because GPEs prevents the shortage while acting as a charge carrier medium.

3.2.5 Electrochemical Characterization

The ionic conductivity of the GPEs was carried out by measuring the EIS using the stainless steel (StSt)/GPE/StSt configuration. The thickness of the GPE film was measured through the use of a digital micrometer (PITTSBURGH). The EIS test was implemented by using the electrochemical workstation (VersaSTAT4), where it was scanned in the range from 10 Hz to 1 Mhz with a scan rate of 25 mV. To evaluate the electrochemical stability of GPEs, the LSV and CV were carried out with the full-cell composed of LFP/GPE/LTO configuration. In the LSV, applied voltage was changed from 0 to 6 V at a sweep rate of 5 mV/s. For the CV test, the voltage range was selected to be from 0 to 3 V at 0.5 mV/s scanning rate. The galvanostatic charge/discharge cycle stability was tested with a battery analyzer (BT2000, ARBIN). The potential window was set to between 1.2 V-2.4 V (versus LTO) for the cycles with current density of 0.1 C (in respect to the theoretical capacity of LFP of 170 mAh/g).

3.3 Results and Discussion

3.3.1 Material Properties

It has been reported that the ternary system using PEGDA/succinonitril (SCN)/LiTFSI demonstrated significant improvement on the ionic conductivity and electrochemical stability. [35, 36] The prepolymer PEGDA was not only able to dissolve the lithium salt and completely mix with plasticizer also the mechanically robust polymer can be formed by UV-crosslinking. To develop a stable polymer electrolyte to the moisture and air, which enables assembly in the open-space, the PEGDA as well as PC and LiTFSI were selected since PC has high boiling and flash points, low toxicity and, is relatively easy to handle. Also, the LiTFSI has high solubility in the PC with high ionic conductivity for the polymer electrolytes.

The thermal stability of GPEs, which is an important factor for resolving the safety issues in batteries, was determined from TGA. Figure 3.1 shows the weight % versus temperature for all of components in GPEs obtained using TGA under nitrogen environment. On the basis of the TGA result, it is apparent that GPEs did not undergo thermal decomposition until about 100 ℃, indicating that the upper limit temperature for the GPEs is 100 ℃. From the data presented in Figure 3.1 (a), the first weight loss for GPEs is attributed to the loss of PC. In comparison with the commonly employed organic carbonate-based electrolytes that exhibited poor thermal stability below 100 ℃, [37] the GPE film could serve as an alternative to provide a safer barrier against conditions at higher temperatures. The second and third weight loss are, respectively, due to decomposition of LiBOB, and PEGDA and LiTFSI. In Figure 3.1 (b), composition 1 shows the highest thermal stability but

composition 6 represents the lowest stability, corresponding to the polymer and plasticizer, which was coherent with the mixing ratio.

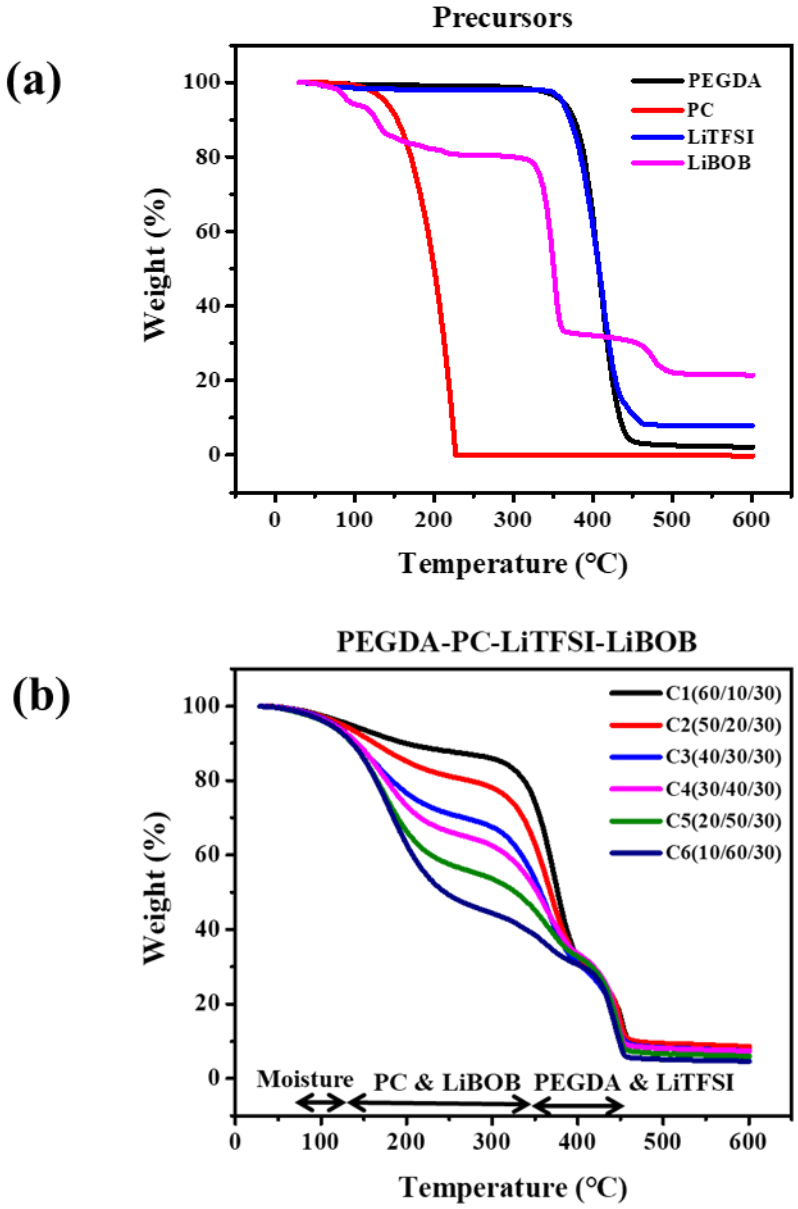

Figure 3. 1 TGA thermogram of (a) the precursors and (b) GPEs prepared in different composition

The crystallinity and amorphousness nature of the GPE were evaluated by the DSC measurements, as shown in Figure 3.2. A melting peak at 17 ℃ is observed for PEGDA while LiTFSI, PC and LiBOB show their T_g at ~ 50 ℃ and 160 ℃, respectively. When PC plasticizer introduced to the PEGDA polymer, the endothermic peaks significantly reduced, indicating the amorphous nature of the polymers in the GPEs. However, as PC plasticizer increase, the glass transition peaks appeared at around 200 ℃, suggesting that the GPE turns from solid-state to more gel-like status.

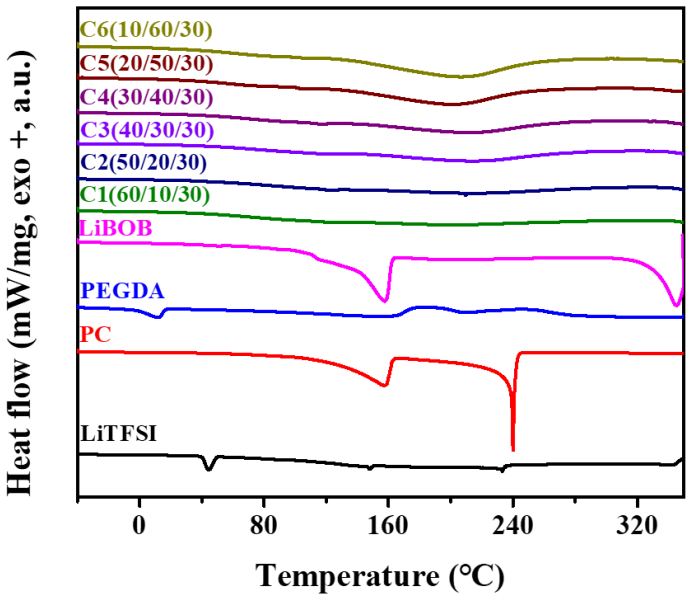

Figure 3. 2 DSC thermograms of precursors and GPEs

In addition to the DSC measurements, the crystallinity of GPEs were confirmed by using the XRD as presented in Figure 3.3. After the PC incorporated into the polymer matrix, the sharp peaks of lithium salts were disappeared or broadened, demonstrating that the added LiTFSI and LiBOB have well dissolved into the GPE matrix. All of them exhibit the XRD peaks from 13 to 30º, indicating that GPEs also present a semi-crystalline structure, and the sharp and narrow peaks observed at ~16.5º and 30.0º are the crystalline peaks of LiBOB salts. [36] The broad peaks at ~21º represent the amorphous phase of the cross-linked PEGDA. Both the DSC and XRD results demonstrate that the crystallinity of GPE can be hindered by the addition of plasticizer of PC. It is anticipated that the amorphous phase of GPEs would help achieve higher ionic conductivity.

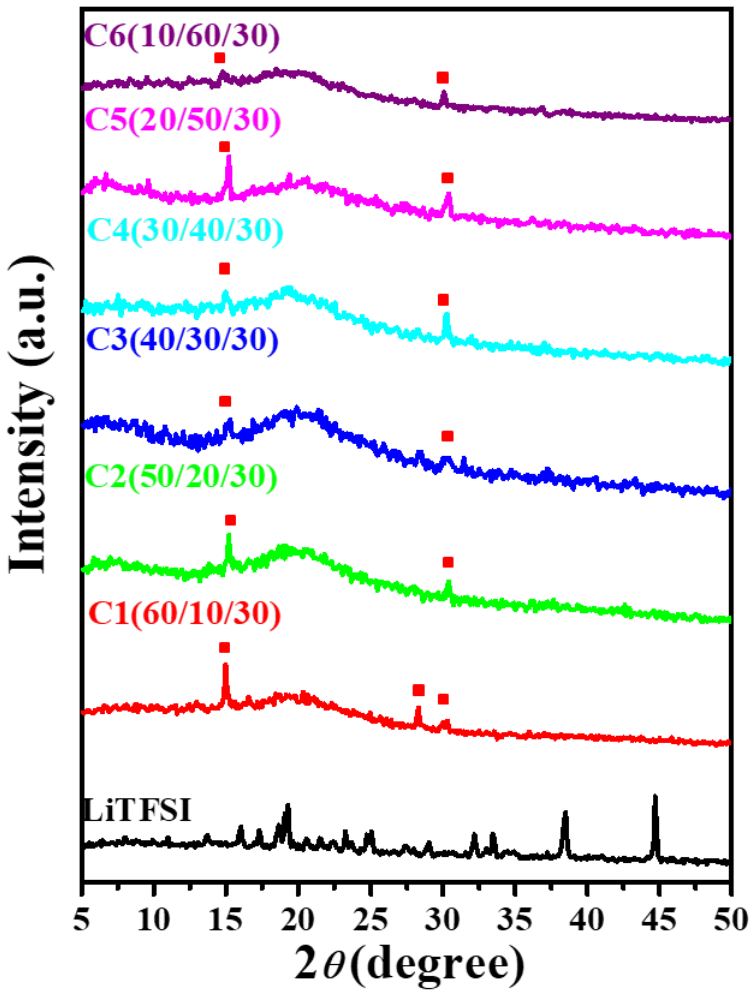

Figure 3. 3 XRD patterns of precursors and GPEs prepared in different composition

3.3.2 Electrochemical Properties

The GPEs prepared by different formulations was studied for the lithium ionic conductivities by the EIS as discussed in Chapter 2. The ionic conductivity of different samples at RT were measured and the Nyquist plot was plotted in Figure 3.4, and summarized in Table 3.2. To determine the resistance value, the X-axis of Nyquist plot was selected at high frequency as shown in the inset figure in Figure 3.4. The highest average ionic conductivities were 3.45 S/cm, that is comparable to the liquid electrolyte (~ 10^{-3} S/cm). It is notable that the increased PC and decreased PEGDA polymer contents give higher ionic conductivities to the GPEs.

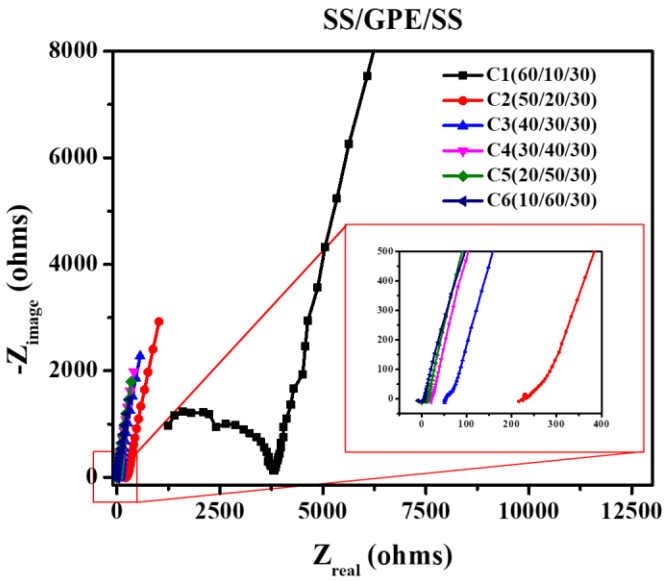

Figure 3. 4 Nyquist plots for GPEs with different formulations

Table 3. 2 Room temperature ionic conductivity for different GPE formulations

Composition	Thickness (cm)	Area (cm^2)	R (Ω)	Ionic conductivity (S/cm)
1	0.1	1.89	2194	2.41×10^{-5}
2	0.104	1.89	409.484	1.34×10^{-4}
3	0.0972	1.89	191.464	2.67×10^{-4}
4	0.134	1.89	40.077	1.77×10^{-3}
5	0.1	1.89	22.073	2.40×10^{-3}
6	0.121	1.89	8.789	7.23×10^{-3}

The first three cycles of CV curves for LFP/GPE/LTO full-cell configuration for the GPE composition of (a) C1, (b) C2, (c) C3, (d) C4, (e) C5, and (f) C6 were represented in Figure 3.5 and Figure 3.6. It is observed that there are three irreversible side reactions taken place at ~ 1.5V, ~ 2 V, and ~ 2.6 V during the oxidation of anodic current, which results from the reaction between the electrolyte and LFP cathode. Specifically, the first reaction was severely consumed in the composition C1, C2, C3, and C4 because the oxidation cannot obtain its first oxidation peak while C5 and C6 relatively achieve the reversible redox reaction. This is because the GPE without the certain amount of PC cannot provide with the Li-ions transport at room temperature instead the Li-ions in PC liquid phase are consumed rapidly near the electrode surface. Moreover, as shown in Figure 3.7, the LSV test demonstrates that the electrochemical stability of electrolyte, C1, shows the decomposition of electrolyte over 1 V, which leading to the side reaction and loss of capacity for the cell.

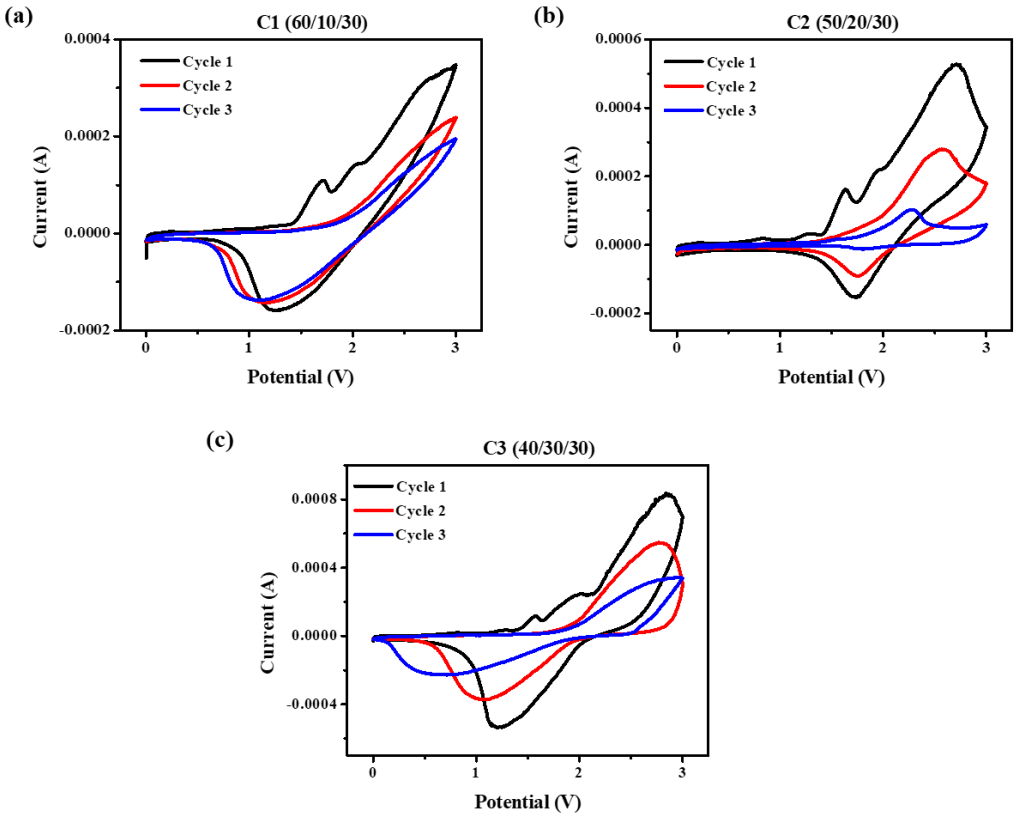

Figure 3. 5 CV for GPEs with different composition in (a) C1(60/10/30) (b) C2(50/20/30), and (c) C3(40/30/30/)

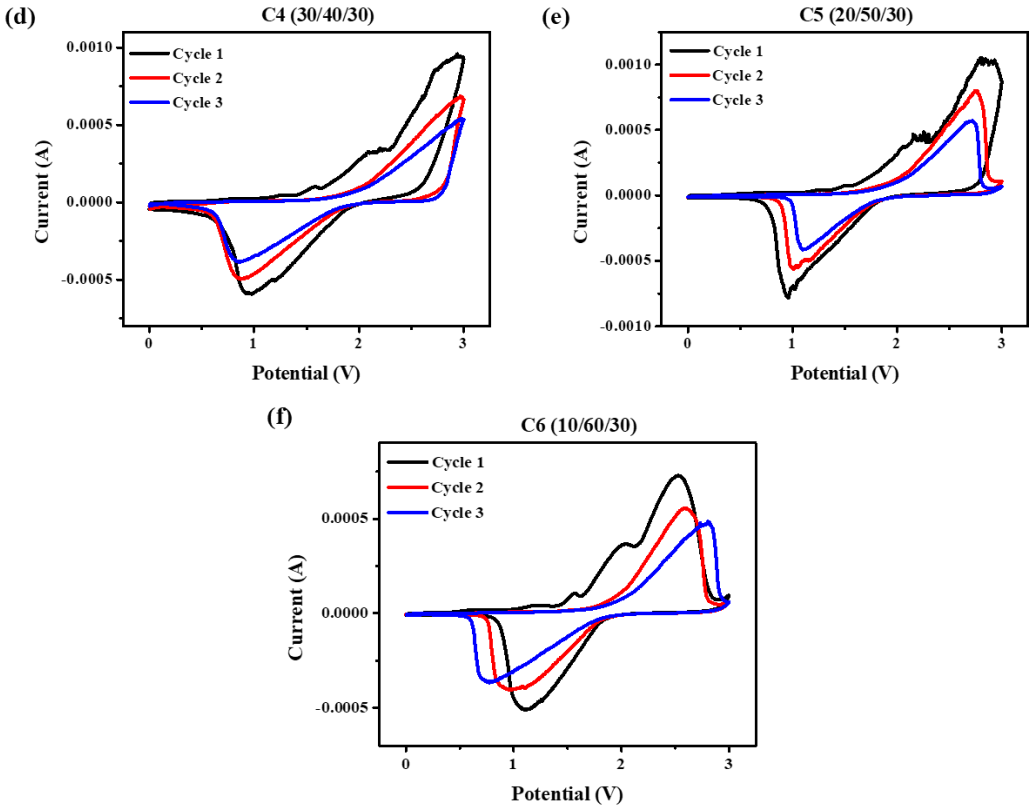

Figure 3. 6 CV for GPEs with different composition in (d) C4(30/40/30) (e) C5(20/50/30), and (f) C6(10/60/30/)

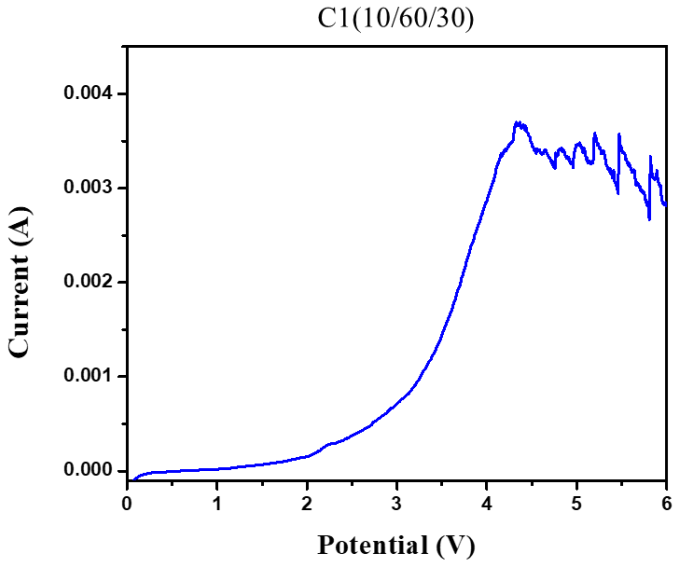

Figure 3. 7 LSV curve for LFP/GPE/LTO cell with C1

The GPE performance was characterized for rate capability in full LFP/LTO cells. These cells were assembled without a separator. Rate capability was done in first charging and discharging cycle at 0.1 C rate. As Figure 3.8 represents, it exhibited a charge capacity of 64 mAh/g, 86 mAh/g, 98 mAh/g, 100 mAh/g, 154 mAh/g, and 103 mAh/g for C1, C2, C3, C4, C5, and C6 while a discharge capacity was measured as 27 mAh/g, 42 mAh/g, 35 mAh/g, 42 mAh/g, 69 mAh/g and 38 mAh/g for C1, C2, C3, C4, C5, and C6. It shows that the C5 exhibits the highest charging and discharging capacity although the ionic conductivity was 2.10×10^{-3}, which is lower than C6. However, as Figure 3.9 indicates, over 10 cycle, the discharge capacity of all the composition was reached to the near zero, 11 mAh/g, 15 mAh/g, 6 mAh/g, 10 mAh/g, 10 mAh/g and 8 mAh/g for C1, C2, C3, C4, C5, and C6, respectively, while the coulombic efficiency of C1, C2, C3, C4, C5, and C6 show 86% and 91%, 81%, 85%, 77%, and 84%. This indicates that the irreversible charging and discharge process and the instability of electrolyte can cause this rapid capacity fading as demonstrated in the CV and LSV test.

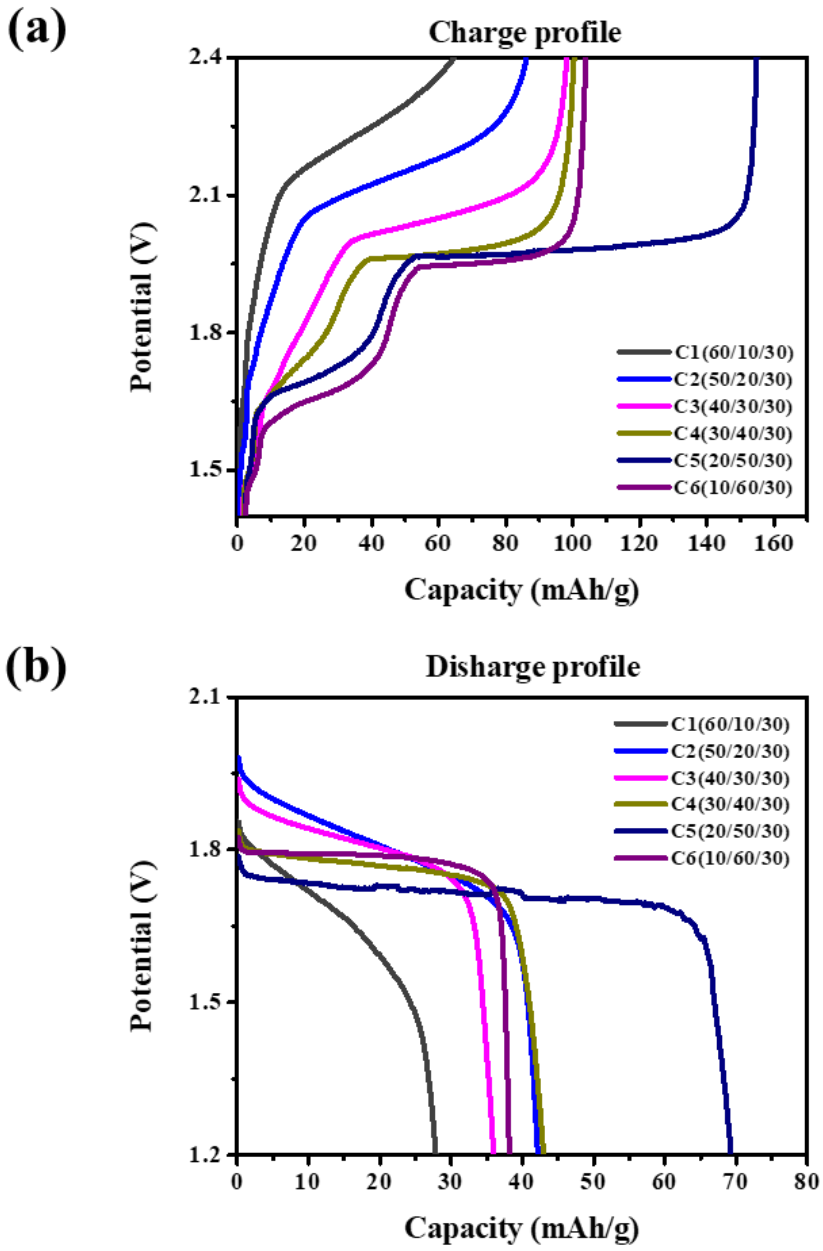

Figure 3. 8 1st cycle of (a) charging and (b) discharging of GPEs

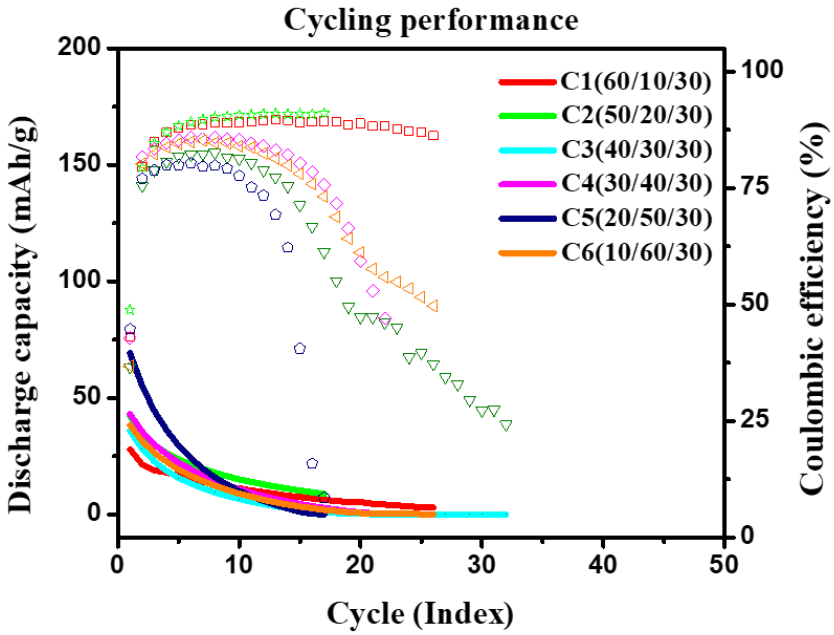

Figure 3. 9 Cycling performance for GPEs

3.3.3 Flammability Test

To evaluate the flammable-resistance of GPEs, a flammable test was performed by igniting the free-standing GPE films with a torch. In the test, it demonstrates that the GPE films resisted burning at first direct contact with the ignition. However, they started to catch a fire within 6 seconds, and completely burn out in 30 sec. There was no recognizable difference between the compositions. However, it is impressive that the pristine PC and PEGDA that possess a flash point of 132 ℃ and 230 ℃, respectively, didn't catch a fire even with the constant contact with the ignition. The flammability of GPEs may be the result from the UV-crosslinking of PEGDA, and the additional experiment will be updated.

From the flammability test, it implies that the GPE can avoid the immediate burning by the first contact of ignition, which means an improvement of safety characteristics for the LIB full-cell.

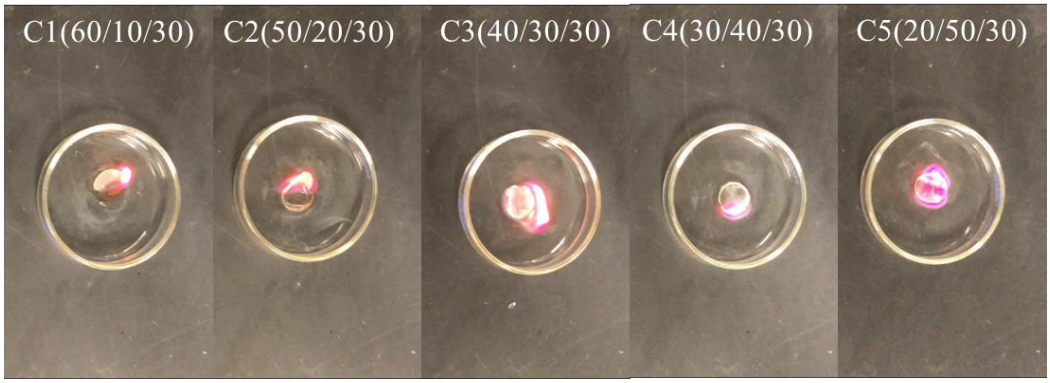

Figure 3. 10 Flammability test for GPEs

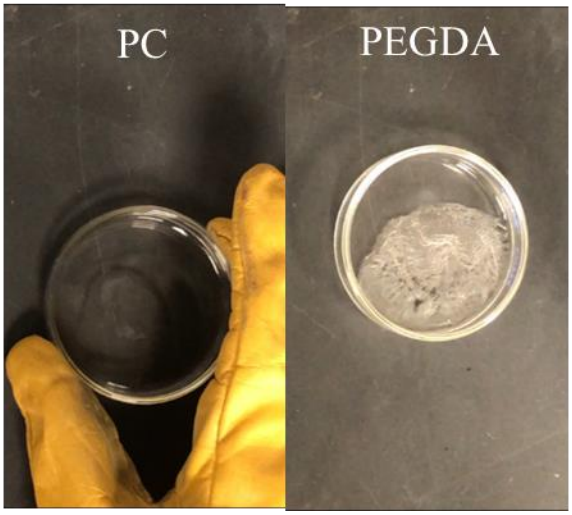

Figure 3. 11 Flammability test for PC and PEGDA

3.4 Conclusion

In conclusion, this research demonstrates a facile and cost-effective fabrication approach for safe, environmentally and thermally stable, and robust gel polymer electrolytes for the full-cell battery. By varying the composition between the PEO, PC, and LiTFSI, it is investigated that the effect of polymer host and plasticizer for the thermal and electrochemical properties of the modified GPEs. Moreover, it is recognized that the research approach presented here, the full-cell fabrication, especially in completely ambient conditions, to improve its safety perspective has been reported for the first time, to the best knowledge. Although the battery performance couldn't reach reasonable battery performance in Chapter 3, the efforts to develop a safe full-cell tolerant to the moisture and air can provide with inspiration as a unique approach. Another effort to improve the battery performance for the safe full-cell battery will be discussed in Chapter 4.

Reference

[1] J. B. Goodenough, “Evolution of strategies for modern rechargeable batteries,” *Acc. Chem. Res.*, vol. 46, no. 5, pp. 1053–1061, 2013, doi: 10.1021/ar2002705.

[2] X. Lu, M. Yu, G. Wang, Y. Tong, and Y. Li, “Flexible solid-state supercapacitors: Design, fabrication and applications,” *Energy Environ. Sci.*, vol. 7, no. 7, pp. 2160–2181, 2014, doi: 10.1039/c4ee00960f.

[3] P. G. Bruce, B. Scrosati, and J. M. Tarascon, “Nanomaterials for rechargeable lithium batteries,” *Angew. Chemie - Int. Ed.*, vol. 47, no. 16, pp. 2930–2946, 2008, doi: 10.1002/anie.200702505.

[4] H. Chen, T. N. Cong, W. Yang, C. Tan, Y. Li, and Y. Ding, “Progress in electrical energy storage system: A critical review,” *Prog. Nat. Sci.*, vol. 19, no. 3, pp. 291–312, 2009, doi: 10.1016/j.pnsc.2008.07.014.

[5] S. Bashir, P. Hanumandla, H. Y. Huang, and J. L. Liu, “Nanostructured materials for advanced energy conversion and storage devices: Safety implications at end-of-life disposal,” *Nanostructured Mater. Next-Generation Energy Storage Convers. Fuel Cells*, vol. 4, no. May, pp. 517–542, 2018, doi: 10.1007/978-3-662-56364-9_18.

[6] B. Scrosati, J. Hassoun, and Y. K. Sun, “Lithium-ion batteries. A look into the future,” *Energy Environ. Sci.*, vol. 4, no. 9, pp. 3287–3295, 2011, doi: 10.1039/c1ee01388b.

[7] G. L. Soloveichik, “Battery technologies for large-scale stationary energy storage,” *Annu. Rev. Chem. Biomol. Eng.*, vol. 2, pp. 503–527, 2011, doi: 10.1146/annurev-chembioeng-061010-114116.

[8] J. Wen, Y. Yu, and C. Chen, “A review on lithium-ion batteries safety issues: Existing problems and possible solutions,” *Mater. Express*, vol. 2, no. 3, pp. 197–212, 2012, doi: 10.1166/mex.2012.1075.

[9] K. Liu, Y. Liu, D. Lin, A. Pei, and Y. Cui, “Materials for lithium-ion battery safety,” *Sci. Adv.*, vol. 4, no. 6, 2018, doi: 10.1126/sciadv.aas9820.

[10] S. Tang, W. Guo, and Y. Fu, “Advances in Composite Polymer Electrolytes for Lithium Batteries and Beyond,” *Adv. Energy Mater.*, vol. 2000802, pp. 1–29, 2020, doi: 10.1002/aenm.202000802.

[11] G. Homann, L. Stolz, J. Nair, I. C. Laskovic, M. Winter, and J. Kasnatscheew, “Poly(Ethylene Oxide)-based Electrolyte for Solid-State-Lithium-Batteries with High Voltage Positive Electrodes: Evaluating the Role of Electrolyte Oxidation in

Rapid Cell Failure," *Sci. Rep.*, vol. 10, no. 1, pp. 2–10, 2020, doi: 10.1038/s41598-020-61373-9.

[12] S. Cho, S. Kim, W. Kim, S. Kim, and S. Ahn, "All-solid-state lithium batteryworking without an additional separator in a polymeric electrolyte," *Polymers (Basel).*, vol. 10, no. 12, pp. 1–16, 2018, doi: 10.3390/polym10121364.

[13] Q. Zhao, S. Stalin, C. Z. Zhao, and L. A. Archer, "Designing solid-state electrolytes for safe, energy-dense batteries," *Nat. Rev. Mater.*, vol. 5, no. 3, pp. 229–252, 2020, doi: 10.1038/s41578-019-0165-5.

[14] Z. Gadjourova, Y. G. Andreev, D. P. Tunstall, and P. G. Bruce, "Ionic conductivity in crystalline polymer electrolytes - Gadjourova et al. - 2001," *Nature*, vol. 412, no. August, pp. 2–5, 2001.

[15] S. K. Fullerton-Shirey and J. K. Maranas, "Effect of LiClO 4 on the structure and mobility of PEO-based solid polymer electrolytes," *Macromolecules*, vol. 42, no. 6, pp. 2142–2156, 2009, doi: 10.1021/ma802502u.

[16] C. Berthier, W. Gorecki, M. Minier, M. B. Armand, J. M. Chabagno, and P. Rigaud, "Microscopic investigation of ionic conductivity in alkali metal salts-poly(ethylene oxide) adducts," *Solid State Ionics*, vol. 11, no. 1, pp. 91–95, 1983, doi: 10.1016/0167-2738(83)90068-1.

[17] Y. Wang and W. H. Zhong, "Development of electrolytes towards achieving safe and high-performance energy-storage devices: A review," *ChemElectroChem*, vol. 2, no. 1, pp. 22–36, 2015, doi: 10.1002/celc.201402277.

[18] S. Cheng, D. M. Smith, and C. Y. Li, "How does nanoscale crystalline structure affect ion transport in solid polymer electrolytes?," *Macromolecules*, vol. 47, no. 12, pp. 3978–3986, 2014, doi: 10.1021/ma500734q.

[19] X. Qian, N. Gu, Z. Cheng, X. Yang, E. Wang, and S. Dong, "Plasticizer effect on the ionic conductivity of PEO-based polymer electrolyte," *Mater. Chem. Phys.*, vol. 74, no. 1, pp. 98–103, 2002, doi: 10.1016/S0254-0584(01)00408-4.

[20] S. Das and A. Ghosh, "Effect of plasticizers on ionic conductivity and dielectric relaxation of PEO-LiClO4 polymer electrolyte," *Electrochim. Acta*, vol. 171, pp. 59–65, 2015, doi: 10.1016/j.electacta.2015.04.178.

[21] E. Quartarone and P. Mustarelli, "Electrolytes for solid-state lithium rechargeable batteries: Recent advances and perspectives," *Chem. Soc. Rev.*, vol. 40, no. 5, pp. 2525–2540, 2011, doi: 10.1039/c0cs00081g.

[22] X. L. Wu, S. Xin, H. H. Seo, J. Kim, Y. G. Guo, and J. S. Lee, “Enhanced Li+ conductivity in PEO-LiBOB polymer electrolytes by using succinonitrile as a plasticizer,” *Solid State Ionics*, vol. 186, no. 1, pp. 1–6, 2011, doi: 10.1016/j.ssi.2011.01.010.

[23] I. Rey, J. C. Lassègues, J. Grondin, and L. Servant, “Infrared and Raman study of the PEO-LiTFSI polymer electrolyte,” *Electrochim. Acta*, vol. 43, no. 10–11, pp. 1505–1510, 1998, doi: 10.1016/S0013-4686(97)10092-5.

[24] R. He, M. Echeverri, D. Ward, Y. Zhu, and T. Kyu, “Highly conductive solvent-free polymer electrolyte membrane for lithium-ion batteries: Effect of prepolymer molecular weight,” *J. Memb. Sci.*, vol. 498, pp. 208–217, 2016, doi: 10.1016/j.memsci.2015.10.008.

[25] L. F. Li *et al.*, “Studies on the enhancement of solid electrolyte interphase formation on graphitized anodes in LiX-carbonate based electrolytes using Lewis acid additives for lithium-ion batteries,” *J. Power Sources*, vol. 189, no. 1, pp. 539–542, 2009, doi: 10.1016/j.jpowsour.2008.10.063.

[26] B. Scrosati and J. Garche, “Lithium batteries: Status, prospects and future,” *J. Power Sources*, vol. 195, no. 9, pp. 2419–2430, 2010, doi: 10.1016/j.jpowsour.2009.11.048.

[27] M. S. Whittingham, “Lithium batteries and cathode materials,” *Chem. Rev.*, vol. 104, no. 10, pp. 4271–4301, 2004, doi: 10.1021/cr020731c.

[28] D. Choi *et al.*, “Li-ion batteries from LiFePO4 cathode and anatase/graphene composite anode for stationary energy storage,” *Electrochem. commun.*, vol. 12, no. 3, pp. 378–381, 2010, doi: 10.1016/j.elecom.2009.12.039.

[29] D. C. T. Xu, W. Wang, M.L. Gordin, D. Wang, “2010_Xu,Wang,Choi-LIB for stationary energy storage.pdf.” p. 62, 2010.

[30] M. Holzapfel, F. Alloin, and R. Yazami, “Calorimetric investigation of the reactivity of the passivation film on lithiated graphite at elevated temperatures,” *Electrochim. Acta*, vol. 49, no. 4, pp. 581–589, 2004, doi: 10.1016/j.electacta.2003.09.012.

[31] X. Sun, P. V. Radovanovic, and B. Cui, “Advances in spinel Li4Ti5O12 anode materials for lithium-ion batteries,” *New J. Chem.*, vol. 39, no. 1, pp. 38–63, 2015, doi: 10.1039/c4nj01390e.

[32] Z. Chen, I. Belharouak, Y. K. Sun, and K. Amine, “Titanium-based anode materials for safe lithium-ion batteries,” *Adv. Funct. Mater.*, vol. 23, no. 8, pp. 959–969, 2013, doi: 10.1002/adfm.201200698.

[33] M. S. Balogun *et al.*, "A review of the development of full cell lithium-ion batteries: The impact of nanostructured anode materials," *Nano Res.*, vol. 9, no. 10, pp. 2823–2851, 2016, doi: 10.1007/s12274-016-1171-1.

[34] A. J. Smith, J. C. Burns, D. Xiong, and J. R. Dahn, "Interpreting High Precision Coulometry Results on Li-ion Cells," *J. Electrochem. Soc.*, vol. 158, no. 10, p. A1136, 2011, doi: 10.1149/1.3625232.

[35] P. Raut, S. Li, Y. M. Chen, Y. Zhu, and S. C. Jana, "Strong and Flexible Composite Solid Polymer Electrolyte Membranes for Li-Ion Batteries," *ACS Omega*, vol. 4, no. 19, pp. 18203–18209, 2019, doi: 10.1021/acsomega.9b00885.

[36] M. Echeverri, C. Hamad, and T. Kyu, "Highly conductive, completely amorphous polymer electrolyte membranes fabricated through photo-polymerization of poly(ethylene glycol diacrylate) in mixtures of solid plasticizer and lithium salt," *Solid State Ionics*, vol. 254, pp. 92–100, 2014, doi: 10.1016/j.ssi.2013.10.050.

[37] C. Arbizzani, G. Gabrielli, and M. Mastragostino, "Thermal stability and flammability of electrolytes for lithium-ion batteries," *J. Power Sources*, vol. 196, no. 10, pp. 4801–4805, 2011, doi: 10.1016/j.jpowsour.2011.01.068.

CHAPTER 4. MODIFICATION OF THE GEL POLYMER ELECTROLYTE FOR THE SAFE FULL CELL

4.1 Introduction

Even though LIBs possesses a high energy and power density, the safety of LIBs is one of the biggest concerns in the research and development of LIBs. One of the main factor of the safety concerns associated with LIBs has been the organic liquid electrolyte that consists of flammable, highly reactive, and corrosive salts and solvents. [1–5] Solid-state electrolytes (SSEs) have been considered one of the promising approaches to replace the liquid electrolyte because of their excellent performances in durability, materials safety, and flexibility as shown in Figure 4.1. [6–8]

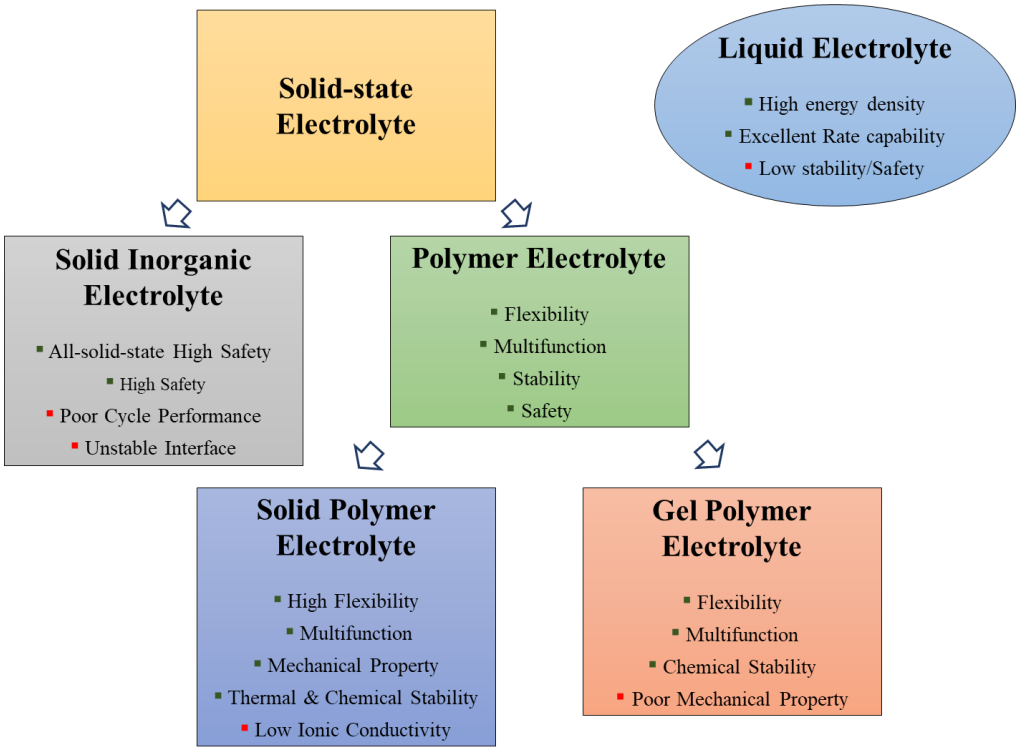

Figure 4. 1 Illustration of the different electrolytes in LIBs [8]

Among diverse SSEs, the solid polymer electrolyte (SPE) is of particular interest due to their superior mechanical/chemical durability and low fabrication cost. PEO is widely researched polymer for the solid-state electrolyte in LIBs, which has the repeated chemical structure of $-CH_2-CH_2-O-$ in its backbone of polymer chain. [9] The PEO has suitable characteristics as a Li^+ ion transporting medium because oxygen in the backbone is electron donating and the polymer chain is flexible. [10, 11] However, due to the semicrystalline nature of PEO, the SPE based on PEO usually shows relatively low ionic conductivity in the range of ~ 10^{-8} to 10^{-4} S/cm at room temperatures, which hinder to be employed for practical LIB applications, compared to that of the liquid electrolyte used in the commercial

LIBs (~ 10^{-3} S/cm). [12–15] The low ionic conductivity of the SPE, which is PEO-Li salt system, is attributed to the poor motion of the polymer segment caused by the crystalline region of PEO polymer host while the relatively fast ion transport takes places in the amorphous region.[8]

To enhance the ionic conductivity at room temperature, it is a common and effective way adding liquid plasticizers such as aprotic organic solvents. The organic solvents such as EC, PC can be added into the polymer host in the SPE system, and it typically results in the formation of gel-like electrolytes , which is called GPE. [16, 17] Plasticization, the introduction of organic solvent into the polymer, results in a large conductivity increase due to the ability of plasticizer to decrease the crystallinity of polymer and increase the mobility of ions in the electrolyte, and the good miscibility with the amorphous PEO-Li-salt complex. [18] This is because plasticizer have relatively high permittivity compared to polymer, and can also enhance the dissociation of ion pairs of salts. The increased amorphous region of PEO by plasticizer with dissolved Li-salts in the GPE can lead to significantly improved ionic conduction. [19–21]

In addition, gel GPEs combine the advantages of liquid electrolyte such as high ionic conductivity and solid polymer electrolyte such as good mechanical properties. [22, 23] Typically, GPEs are prepared by a polymer or mixture of polymer host, plasticizer, and lithium salts followed by casting, rolling, or curing (e.g., UV or thermal triggers) process. [19,24–27] In the SPEs, Li-ions transport through hopping from one site to other by the segmental motion of polymer, [8] while the Li-ion transport in GPEs occurs generally in liquid phase trapped within the pores of the host polymer matrix. [28] However, although

the plasticization could significantly improve the ionic conductivity of polymer electrolyte at room temperature, it could also deteriorate the GPEs such as the weakened mechanical rigid and increased reactivity towards the metal electrode. [29–31]

In this respect, inspired by previous work in Chapter 3, we hypothesize that the stability and robustness of GPEs can be greatly improved in combination between the polymer host, lithium salts and plasticizer. In this chapter, it is studied that the development of gel polymer electrolytes based on the PEO-PC-LiTFSI/LiBOB mixture that exhibited resistance to the moisture for the lithium-ion full cell that can be assembled in the ambient condition. In addition, in order to optimize the ionic conductivity of GPE while not losing their mechanical property, the samples are prepared by varying the amount of PC, LiTFSI and LiBOB, respectively, at fixed PEO contents. As well, the physical and chemical properties of the GPEs are characterized in addition to the electrochemical characterizations. For the full cell performance, the GPEs are introduced to LFP and LTO as cathode and anode electrode, respectively, CR2032-coin cell.

4.2. Experimental

4.2.1 Electrolyte Preparation

As described in Chapter 2, at fixed amount of PEO, PC and Li-salt are divided into three sets in 1 M LiTFSI, 0.5 M LiTFSI, and 0.5 M LiBOB while 1 mmol of LiTFSI or 1 mmol LiBOB are used as the major salt with LiBOB or LiTFSI additives in the weight ratio of 0.2, 0.1, 1, and 2 in respect to the weight of total mixture, such as 1 M LiTFSI-LiBOB (major-additive) or 0.5 M LiBOB-LiTFSI (major-additive). The less or more PC contents cannot be used because of either the limited of lithium salts solubility, or the deformation of mechanical strength of electrolyte. Figure 4.2 depicts the chemical structures of the PEO, PC, LiTFSI and LiBOB.

For comparison, a liquid electrolyte, 0.6 m LiBOB dissolved in PC-DEC (1:1 weight ratio) solvent mixture, is selected owing to its highest conductivity of ~ 8.2 x 10^{-3} S/cm as reported by Ding et al. [32]

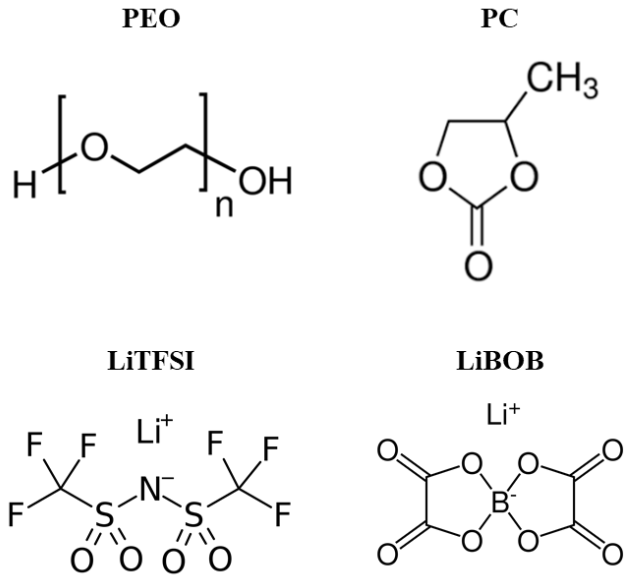

Figure 4. 2 Chemical structures of the GPE components: PEO, PC, LiTFSI and LiBOB

Table 4. 1 Different composition for GPEs

Composition		Weight ratio			
		PEO	PC	LiTFSI	LiBOB
1 M LiTFSI (LiBOB additive)	PT13B0	1	1	3	0
	PT13B0.2	1	1	3	0.2
	PT13B0.5	1	1	3	0.5
	PT13B1	1	1	3	1
	PT13B2	1	1	3	2
0.5 M LiTFSI (LiBOB additive)	PT23B0.2	1	2	3	0.2
	PT23B0.5	1	2	3	0.5
	PT23B1	1	2	3	1
	PT23B2	1	2	3	2
0.5 M LiBOB (LiTFSI additive)	PB22T0	1	2	0	2
	PB22T0.2	1	2	0.2	2
	PB22T0.5	1	2	0.5	2
	PB22T1	1	2	1	2
	PB22T2	1	2	2	2

4.2.2 GPE Characterizations

T_g, T_m, and crystallinity of the GPE film was determined by the utilization of DSC (DSC 214 Polyma, Netzsch), where the temperature range was scanned from -40 to 350 ℃ at a temperature ramping rate of 10 ℃/min. The GPE film samples for the DSC were pre-dried overnight in the fume hood. TGA (TG 209 F1 Libra, Netzsch) was used to determine the weight percentage component of the thermal stability of the GPE. The temperature was measured from 30 to 600 ℃ at a rate of 10 ℃/min under nitrogen atmosphere for the weight percentages of different components. The structural characterization of the GPE was characterized by XRD (Empyrean Series2, PANalytical) with Cu Kα radiation (λ = 1.5406Å) at an accelerating voltage set at 40 kV with 40 mA in the 2θ range of 5 - 50º.

4.2.3 Electrochemical Characterization

The ionic conductivity measurement of the GPE was carried by using the StSt/GPE/StSt configuration. The thickness of the GPE film was measured through the use of a digital micrometer (PITTSBURGH). The EIS was characterized by the potentiostat (VersaSTAT4), where it was scanned in the range of 10 Hz-1 MHz. The CV measurement was carried out with the full-cell composed of LFP/liquid/LTO or LFP/GPE/LTO configuration, where the voltage range was selected to be from 0 to 3 V at a scanning rate of 0.5 mV/s. The galvanostatic charge/discharge cycle stability test for the full-cell was carried out on a battery analyzer (BT2000, ARBIN). The potential window was set to

between 1.2 V-2.4 V (versus LTO) for the cycles with current density of 0.1 C (in respect to the theoretical capacity of LFP of 120 mAh/g).

4.3. Results and Discussion

4.3.1 Material Properties

To evaluate its thermal stability, TGA was carried out for the GPE samples as shown in Figure 4.3. Firstly, PEO, PC, and PEO dissolved in PC (0.2 ml) precursors are characterized in Figure 4.3.a). Although PEO exhibits its thermal durability up to ~ 400 ℃, the decomposition of PC begins at ~ 150 ℃ and it affects to PEO and PC mixture directly. The first weight loss of PEO mixture from 120 ℃ to 160 ℃ is attributed to the moisture , the second weight loss from 360 ℃ to 400 ℃ is related to the PC & LiBOB, lastly, it is corresponding to PEO & LiTFSI. When 1 M LiTFSI is used to the PEO in Figure 4.3.b), the thermal stability of GPEs can be relatively extended to ~ 150 ℃, compared to the precursors. Especially, PT13B0, without LiBOB additive, the PEO-PC-LiTFSI composition exhibits the best thermal stability among 1 M LiTFSI samples as the first weight loss achieved only 78 % until 400 ℃, because of partially dissolved PEO host and the exceed contents of Li salts. In Figure 4.3.c) and d), it is demonstrated that the first weight loss of 40 % and 50 % from 120 ℃ to 240 ℃, respectively, mainly attributed to the decomposition of PC when the increased amount of PC is used. The other two steps of decomposition can be contributed to the LiBOB, and PEO and LiTFSI from 250 ℃ to

450 ℃. It indicates the improved thermal stability of PEO-based GPEs, compared to the liquid electrolytes.

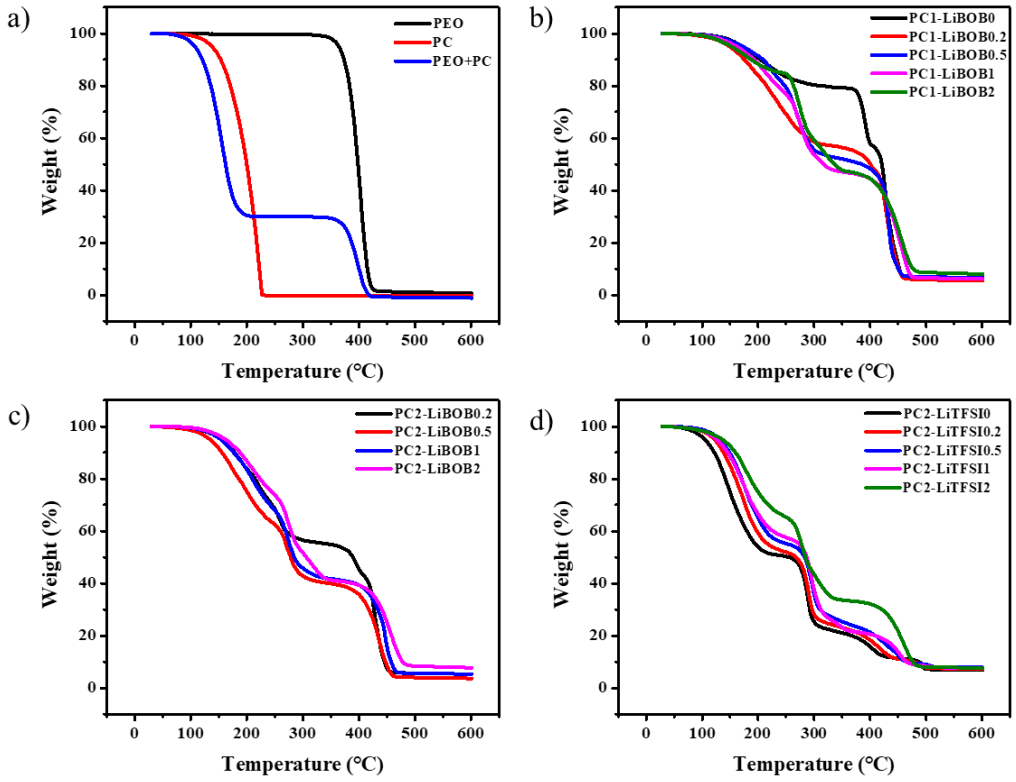

Figure 4. 3 TGA thermogram of a) the precursors and GPEs prepared with b) 1 M LiTFSI-LiBOB, c) 0.5 M LiTFSI-LiBOB, and d) 0.5 M LiBOB-LiTFSI compositions

Figure 4.4 represents the DSC thermogram of the pristine PEO polymer host, PEO dissolved in PC, and GPEs. Although the pristine PEO shows the T_m at 67.3 ℃, it is observed that the T_m of PEO decreased to 36.2 ℃ when the plasticizer was introduced, which indicates the decreased crystalline ratio in the polymer host. The second endothermic peak represents the PC decomposition at around 240 ℃. Figure 4.4.b) and c) represent the

DSC results when the weight ratio of PC is 1 and LiTFSI is used as major salt. In Chapter 3, it exhibits that the first endothermic peak, T_m, of LiBOB appears at 160 °C. It is noticed that the behavior of GPEs is much contributed to the that of LiBOB, as the contents of LiBOB increase. This suggests the lack of PC composition cannot dissolve the LiBOB salts completely. In Figure 4.2.d), the increased PC content shows relatively better dissolution of LiBOB, which leads to the increased amorphous areas, however, the LiBOB salts are still remaining as crystalline solid form. From the DSC results, it suggests that the LiBOB is excessive and not dissolved but the presence of LiBOB may strengthen the mechanical robustness of GPE.

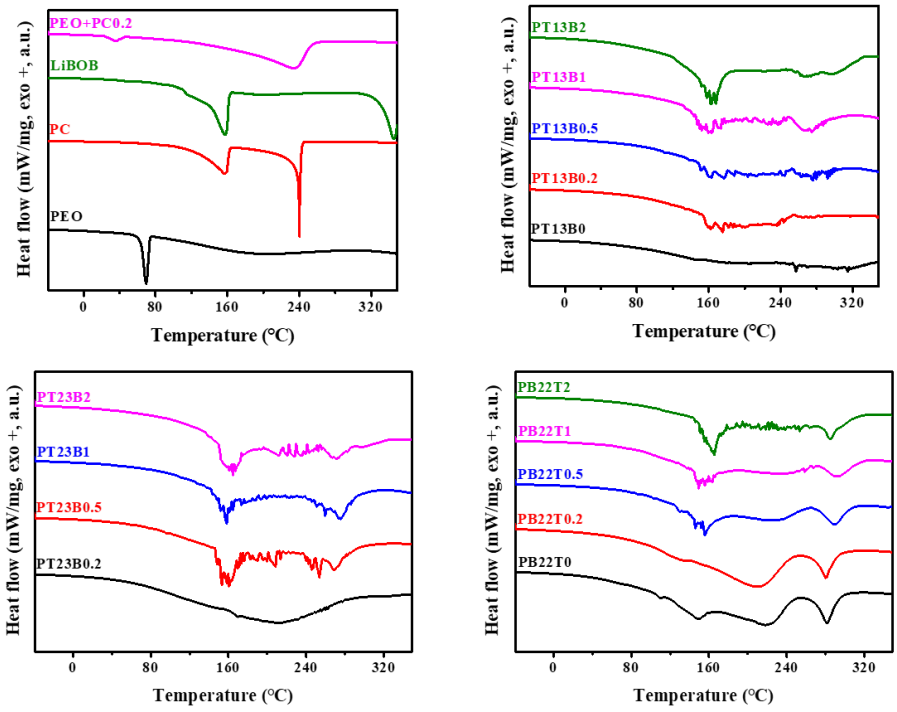

Figure 4. 4 DSC thermograms of a) the precursors and GPEs prepared with b) 1 M LiTFSI-LiBOB, c) 0.5 M LiTFSI-LiBOB, and d) 0.5 M LiBOB-LiTFSI compositions

In addition to DSC, the XRD is measured to confirm the crystallinity of GPEs. As presented in Figure 4.5.a), when the added LiBOB excesses 1 and 2 in weight ratio, the sharp peaks of lithium salts are appeared at 2θ = 19º and 23º, while LiTFSI peaks are not detected. It demonstrates that the 1 mmol of LiTFSI can be dissolved completely but the LiBOB have not dissolved in the weight ratio of 1 of PC. On the other hand, the PC2 samples represents the better dissolution of LiBOB as shown in Figure 4.5.b). When the contents of LiBOB dominate, there is intense peak of PEO-LiBOB appeared at ~ 20º as shown in Figure 4.5.c) while LiTFSI peaks barely detected because of their high solubility.

Both DSC and XRD results demonstrate that the crystallinity of GPE can be hindered by the addition of plasticizer of PC while supporting the mechanical strength of the GPE by the excessive amount of Li salts that possess crystallinity because of not completely dissolved.

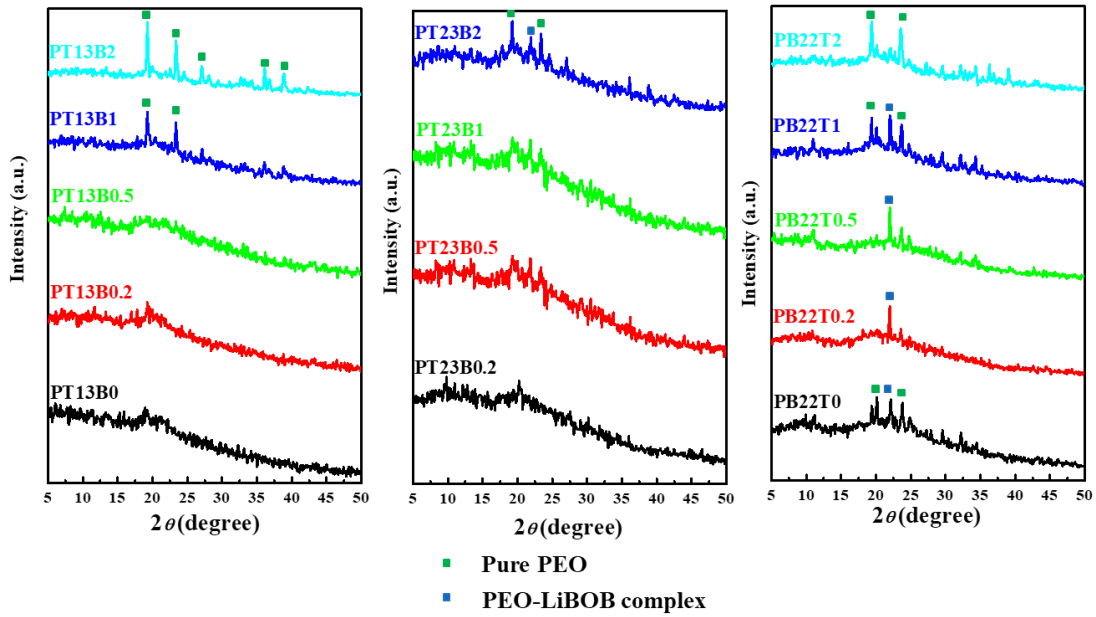

Figure 4. 5 XRD patterns of precursors and GPEs prepared in different composition

4.3.2 Electrochemical Properties

The ionic conductivities of GPEs are measured by the EIS and the results are represented in Nyquist plot as shown in Figure 4.6, and the calculated conductivities are listed in Table 4.2. PT13B0 and PT13B2 show the two lowest ionic conductivities of 6.86 x 10^{-5} and 8.94 x 10^{-5} S/cm, respectively. This may result from the insufficiency of PC that cause the lack of liquid regions where the Li ions transport, and of dissociation of lithium salts ion pairs, compared to PC2-samples. By contrast, the two highest ionic conductivities are 1.01 x 10^{-3} and 9.16 x 10^{-4} S/cm for PB22T1 and PB22T2, respectively. It is suggesting that the proper amount of PC contents can decrease the crystallinity of polymer matrix while increasing the amorphous regions, which results in the increased ionic conductivities.

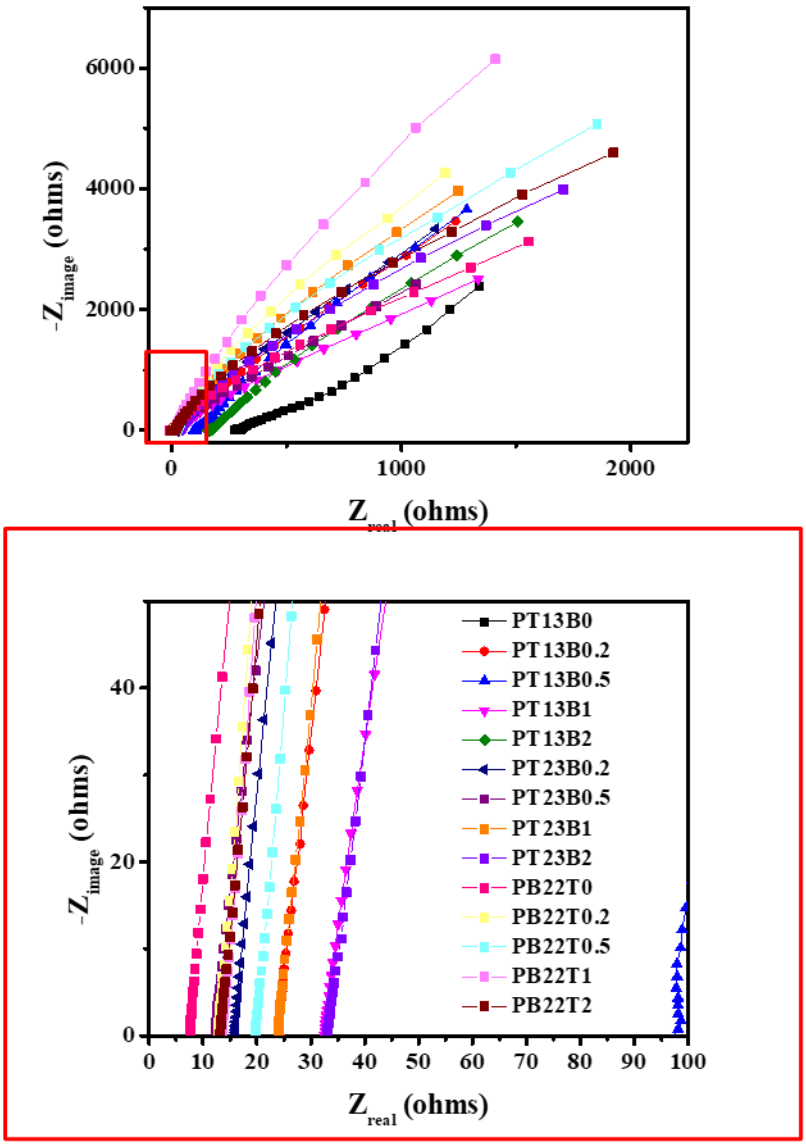

Figure 4. 6 Nyquist plots for GPEs with different formulations

Table 4. 2 Room temperature ionic conductivity for different GPE formulations

Composition	Thickness (cm)	Area (cm^2)	R (Ω)	Ionic conductivity (S/cm)
PT13B0	0.0354	1.77	291.675	6.86×10^{-5}
PT13B0.2	0.0146	1.77	24.084	3.42×10^{-4}
PT13B0.5	0.0385	1.77	98.144	2.22×10^{-4}
PT13B1	0.0089	1.77	32.685	1.54×10^{-4}
PT13B2	0.0266	1.77	168.195	8.94×10^{-5}
PT23B0.2	0.0204	1.77	15.937	7.23×10^{-4}
PT23B0.5	0.0127	1.77	12.299	5.83×10^{-4}
PT23B1	0.0288	1.77	23.99	6.78×10^{-4}
PT23B2	0.0345	1.77	33.202	5.87×10^{-4}
PB22T0	0.0106	1.77	7.608	7.87×10^{-4}
PB22T0.2	0.0145	1.77	12.871	6.36×10^{-4}
PB22T0.5	0.0255	1.77	19.781	7.28×10^{-4}
PB22T1	0.0243	1.77	13.625	1.01×10^{-3}
PB22T2	0.0215	1.77	13.267	9.16×10^{-4}

The CV test was performed for the first three cycles of GPEs using the LFP/GPE/LTO configuration. Overall, it is recognized that there are two oxidation reaction in Cycle 1 for all the composition although either LiTFSI or LiBOB is absent, which may be contributed to the possible oxidation of trace of water, or electrolyte on the LFP cathode. In Figure 4.7, it is represented that the PEO-based GPEs with composition of 1 M LiTIFSI exhibit the reversible redox reaction peaked at ~ 2.4 V and ~ 1.2 V except the first cycle, especially with the weight ratio of LiBOB in 0.2 and 0.5. In Figure 4.8, there are instable reduction reaction on the sample PT23B0.2, PT23B0.5, and PT23B2 while PT23B1 shows unstable oxidation reaction. This behavior is observed on the sample PB22T1 and PB22T2 for their

reduction in Figure 4.9. It may result from the reductive reaction of the excessive amount of PC and LiTFSI but the presence of LiBOB can relief their unstable reaction. When the LiBOB is used as the major lithium salt in the amount such as PB22T0, PB22T0.2, and PB22T0.5, it is observed that there are two oxidative side reactions taken place in cycle 1 and cycle 2.

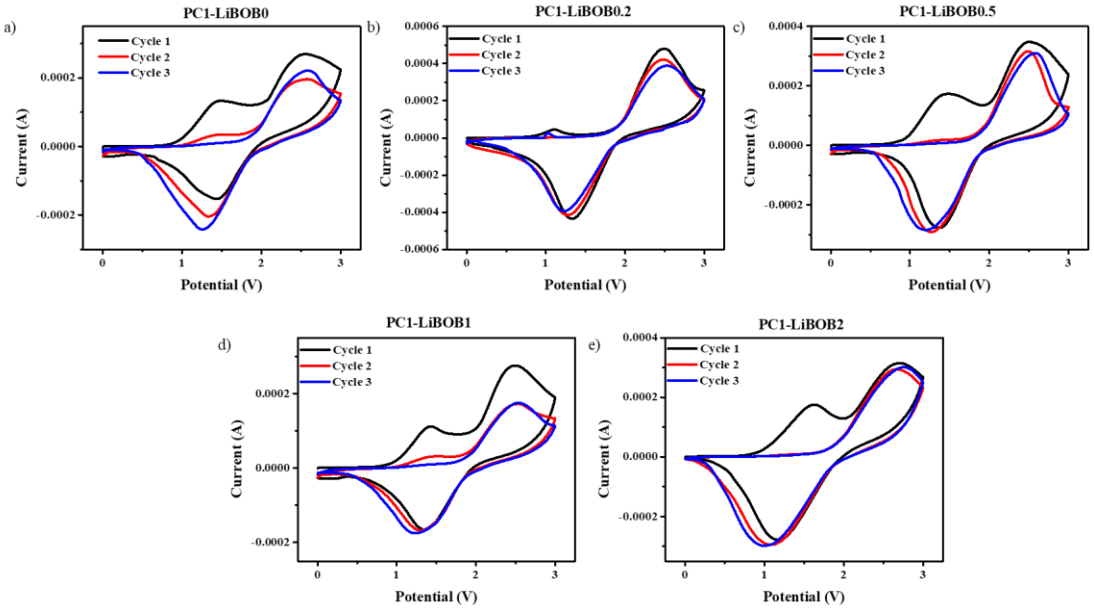

Figure 4. 7 First 3 cycles for GPEs with 1 M LiTFSI composition

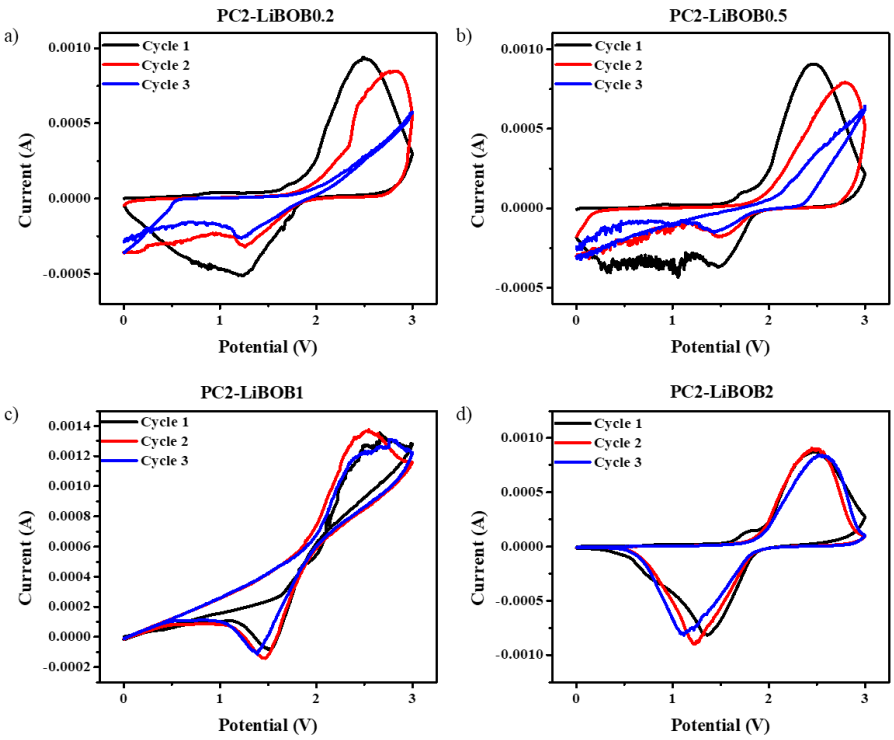

Figure 4. 8 First 3 cycles for GPEs with 0.5 M LiTFSI composition

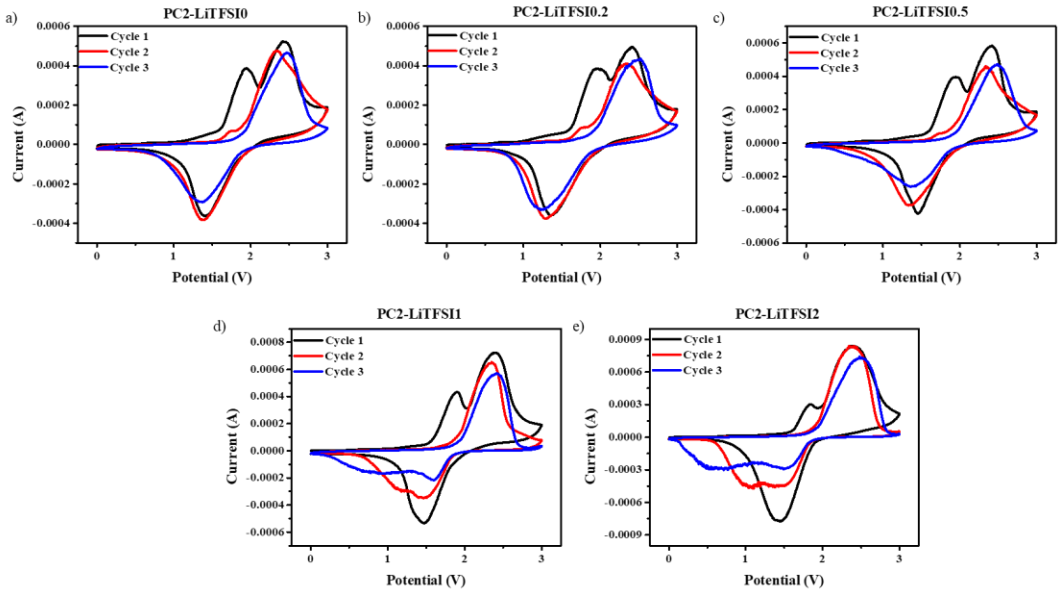

Figure 4. 9 First 3 cycles for GPEs with 0.5 M LiBOB composition

The charge and discharge profile for the first cycle for the GPEs is also investigated to evaluate their capacity. In Figure 4.10.a), the liquid electrolyte, 0.6 m LiBOB, exhibits the charge capacity of 151 mAh/g, but about half of capacity for the discharge is shown as of 82 mAh/g. Meanwhile, PT23B0.2, PT23B0.5, PT23B1, and PT23B2 in Figure 4.10.b) show the better performance in the charge capacity of 126 mAh/g, 126 mAh/g, 149 mAh/g, and 145 mAh/g, respectively, and in the discharge capacity of 86 mAh/g, 86 mAh/g, 109 mAh/g, and 106 mAh/g, with flat charging and discharging plateau. However, even though it exhibited the relatively high ionic conductivity, the GPEs with composition of PB22T0, PB22T0.2, PB22T0.5, PB22T1, and PB22T2 in Figure 4.10.c) represent similar charge capacity as of 103 mAh/g, 139 mAh/g, 139 mAh/g, 141 mAh/g, and 141 mAh/g, respectively, and relatively low discharge capacity as of 60 mAh/g, 53 mAh/g, 61 mAh/g, 62 mAh/g, and 86 mAh/g, respectively.

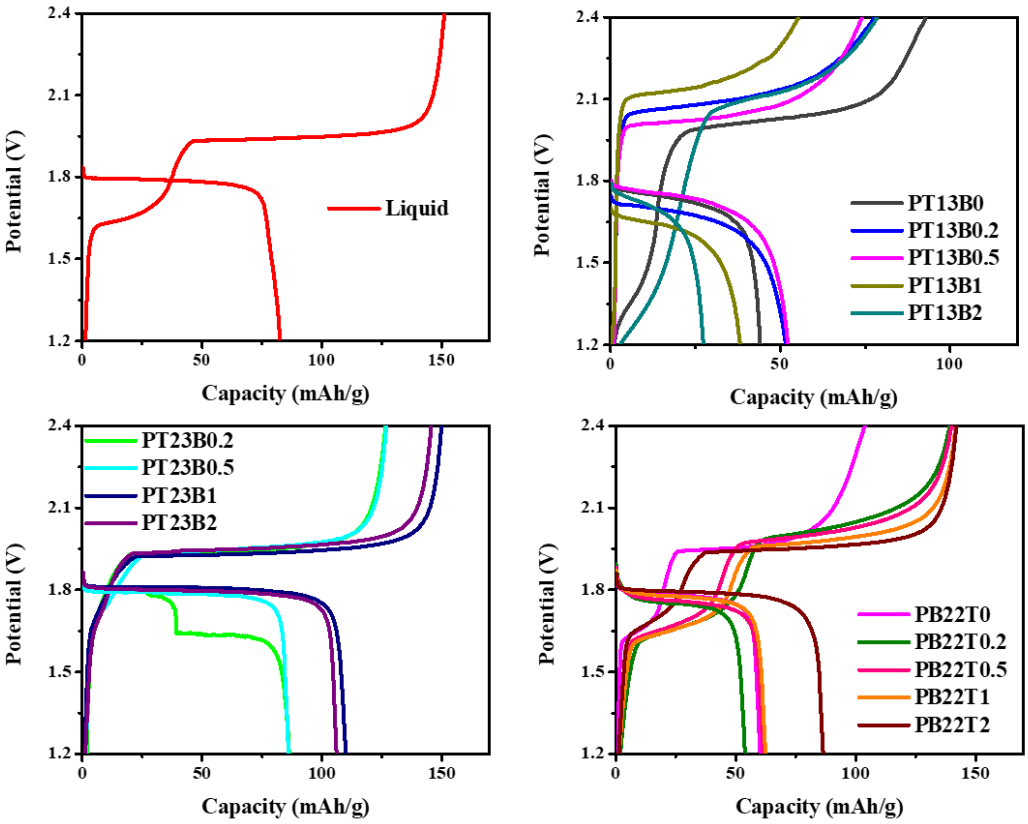

Figure 4. 10 Charge and discharge profile for the 1st cycle of GPEs

In addition, galvanostatic cyclic charging/discharging measurements are performed in LFP/liquid/LTO and LFP/GPE/LTO full cells. For comparison, 0.6 m LiBOB liquid electrolytes is prepared in the open-space and used to CR2032 coin cell. As Figure 4.7.a) shows, the cycling stability of liquid electrolyte shows a rapid capacity fading within 10 cycles. Compared to the blank tests, the GPEs with different composition of PC and lithium

salts demonstrate the relatively high coulombic efficiency and cycling stability. In Figure 4.7.b), the discharge capacities of samples are overall lower than the theoretic capacity of ~ 170 mAh/g. This is because the GPE with PC1 weight ratio cannot properly contact the interface of electrodes properly due to their high crystallinity and low flexibility. Among PC13LiBOB samples, PT13B2 shows the stable cycling performance and high coulombic efficiency of 97.7% over 50 cycles while it records a low discharge capacity of ~ 25 mAh/g. The relatively low capacity of PT13B2 in the beginning of cycles may result from the lowest ionic conductivity as discussed but the intrinsic property of LiBOB, which is the stability for long cycles, caused the stable cycling performance over cycles. In Figure 4.7.c), PT23B0.2 sample is not included since the sample was not working properly, it failed after 2 cycles. The GPEs composed of PC23B samples show the better performance in terms of discharge capacity in this study. It has been cycled over 45, and the discharge capacities are maintained as 24 mAh/g, 40 mAh/g, and 46 mAh/g for PT23B0.5, PT23B1, and PT23B2, respectively while the coulombic efficiency of them maintains 97%, 77%, and 98%, respectively.

The discharge capacities of PB22T0, PB22T0.2, PB22T0.5, PB22T1, and PB22T2 at 50 cycles achieved 53 mAh/g, 0.21 mAh/g, 0.51 mAh/g, 12mAh/g, and 30 mAh/g, with the coulombic efficiency of 98, fluctuated numbers over 100% for PB22T0.2 and PB22T0.5 96, and 98%, respectively. PB22T0 shows the best discharge capacity and coulombic efficiency over 62 cycles, as 50 mAh/g and 98% respectively. This suggests that the presence of LiBOB without LiTFSI in the gel polymer matrix can provide with the more stable and reversible oxidation and reduction reactions between electrolyte and electrodes

with decreased side reactions. It may result from the stability of LiBOB to the moisture while LiTFSI has high reactivity and can be oxidized when exposure to the moisture and air.

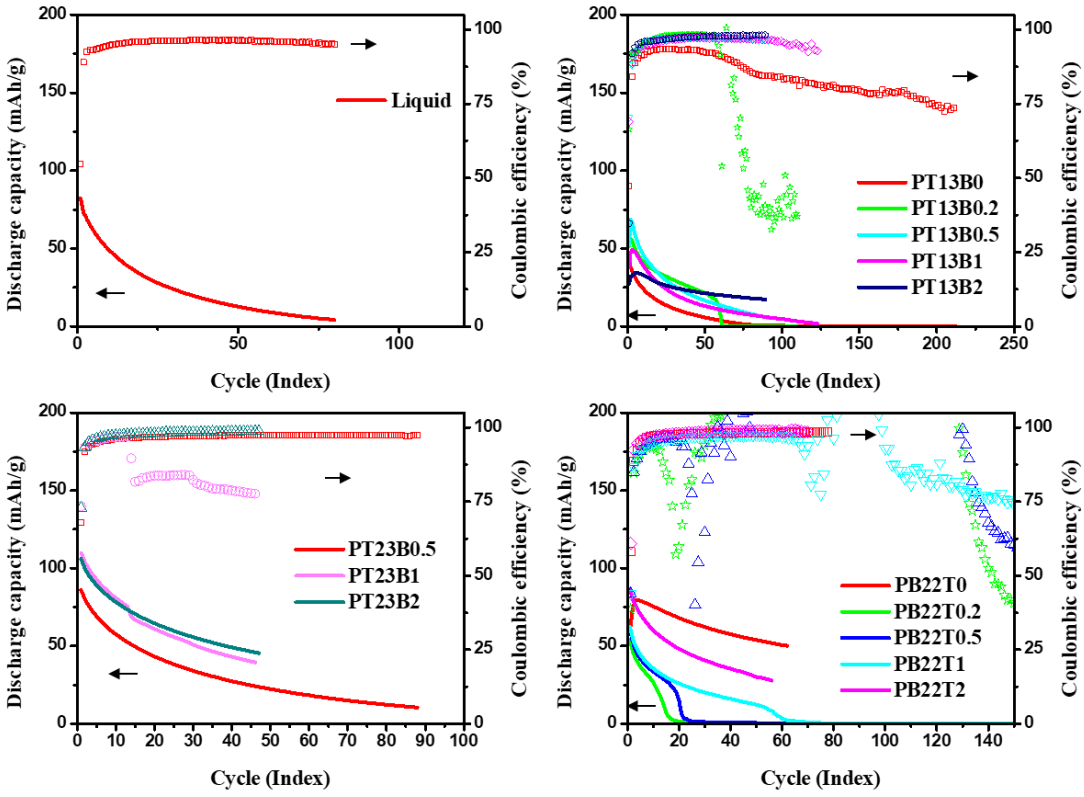

Figure 4. 11 Cycling performance of GPEs

4.4 Conclusion

It is demonstrated that incorporation of lithium dual salts with an organic liquid solvent in a polymer matrix can improve both the electrochemical performances as well as the stability of the electrolytes compared to the liquid electrolyte as a counterpart. Specifically, it demonstrates a rapid synthetic route to a new class of safe and stable PEO-based GPEs when exposure to the moisture, based on a combination of PEO, PC, LiTFSI and LiBOB. For the first time, these gel polymer electrolytes are tested in LIB full cells with LFP/LTO cathode/anode, respectively, assembled in the ambient condition. The GPEs generally exhibit improved electrochemical cyclic stability when LiBOB is used as a major salt compared to when LiTFSI used as a major, as well as to the liquid electrolyte based on LiBOB. Finally, we demonstrate that PEO-based GPEs significantly enhance the cycling performance with enhanced thermal stability due to the compositions, while they are also more tolerable to environmental exposure to the presence of moisture and air when they are prepared. These results imply the potential of this technology for safe, robust, stable Li-ion batteries.

Reference

[1] J. Kalhoff, G. G. Eshetu, D. Bresser, and S. Passerini, "Safer electrolytes for lithium-ion batteries: State of the art and perspectives," *ChemSusChem*, vol. 8, no. 13, pp. 2154–2175, 2015, doi: 10.1002/cssc.201500284.

[2] M. Armand, "Nature Lithium Battery," *Nature*, vol. 414, no. November, pp. 359–367, 2001, [Online]. Available: http://www.ncbi.nlm.nih.gov/pubmed/11713543.

[3] G. L. Woods *et al.*, "A mule cloned from fetal cells by nuclear transfer," *Science (80-.).*, vol. 301, no. 5636, p. 1063, 2003, doi: 10.1126/science.1086743.

[4] R. A. Huggins, "Do You Really Want an Unsafe Battery?," *J. Electrochem. Soc.*, vol. 160, no. 5, pp. A3001–A3005, 2013, doi: 10.1149/2.001305jes.

[5] J. B. Goodenough and Y. Kim, "Challenges for rechargeable Li batteries," *Chem. Mater.*, vol. 22, no. 3, pp. 587–603, 2010, doi: 10.1021/cm901452z.

[6] G. Homann, L. Stolz, J. Nair, I. C. Laskovic, M. Winter, and J. Kasnatscheew, "Poly(Ethylene Oxide)-based Electrolyte for Solid-State-Lithium-Batteries with High Voltage Positive Electrodes: Evaluating the Role of Electrolyte Oxidation in Rapid Cell Failure," *Sci. Rep.*, vol. 10, no. 1, pp. 2–10, 2020, doi: 10.1038/s41598-020-61373-9.

[7] S. Tang, W. Guo, and Y. Fu, "Advances in Composite Polymer Electrolytes for Lithium Batteries and Beyond," *Adv. Energy Mater.*, vol. 2000802, pp. 1–29, 2020, doi: 10.1002/aenm.202000802.

[8] Z. Xue, D. He, and X. Xie, "Poly(ethylene oxide)-based electrolytes for lithium-ion batteries," *J. Mater. Chem. A*, vol. 3, no. 38, pp. 19218–19253, 2015, doi: 10.1039/c5ta03471j.

[9] S. Li *et al.*, "A Superionic Conductive, Electrochemically Stable Dual-Salt Polymer Electrolyte," *Joule*, vol. 2, no. 9, pp. 1838–1856, 2018, doi: 10.1016/j.joule.2018.06.008.

[10] N. K. Karan, O. K. Pradhan, R. Thomas, B. Natesan, and R. S. Katiyar, "Solid polymer electrolytes based on polyethylene oxide and lithium trifluoro- Methane sulfonate (PEO-LiCF3so3): Ionic conductivity and dielectric relaxation," *Solid State Ionics*, vol. 179, no. 19–20, pp. 689–696, 2008, doi: 10.1016/j.ssi.2008.04.034.

[11] W. Gorecki, M. Jeannin, E. Belorizky, C. Roux, and M. Armand, "Physical properties of solid polymer electrolyte PEO(LiTFSI) complexes," *J. Phys. Condens. Matter*, vol. 7, no. 34, pp. 6823–6832, 1995, doi: 10.1088/0953-8984/7/34/007.

[12] H. Yang, G. V. Zhuang, and P. N. Ross, “Thermal stability of LiPF6 salt and Li-ion battery electrolytes containing LiPF6,” *J. Power Sources*, vol. 161, no. 1, pp. 573–579, 2006, doi: 10.1016/j.jpowsour.2006.03.058.

[13] K. Xu, “Electrolytes and interphases in Li-ion batteries and beyond,” *Chem. Rev.*, vol. 114, no. 23, pp. 11503–11618, 2014, doi: 10.1021/cr500003w.

[14] A. Magistris and C. Fisica, “PEO-Based Polymer Electrolytes,” vol. 28, no. March 1990, pp. 277–280, 1992.

[15] C. A. C. Sequeira and D. M. F. Santos, “Polymer Electrolytes: Fundamentals and Applications,” *Polym. Electrolytes Fundam. Appl.*, pp. 1–623, 2010, doi: 10.1533/9781845699772.

[16] S. Das and A. Ghosh, “Effect of plasticizers on ionic conductivity and dielectric relaxation of PEO-LiClO4 polymer electrolyte,” *Electrochim. Acta*, vol. 171, pp. 59–65, 2015, doi: 10.1016/j.electacta.2015.04.178.

[17] K. Mishra, S. S. Pundir, and D. K. Rai, “Effect of polysorbate plasticizer on the structural and ion conduction properties of PEO–NH4PF6 solid polymer electrolyte,” *Ionics (Kiel).*, vol. 23, no. 1, pp. 105–112, 2017, doi: 10.1007/s11581-016-1790-2.

[18] Q. Zhao, S. Stalin, C. Z. Zhao, and L. A. Archer, “Designing solid-state electrolytes for safe, energy-dense batteries,” *Nat. Rev. Mater.*, vol. 5, no. 3, pp. 229–252, 2020, doi: 10.1038/s41578-019-0165-5.

[19] X. Cheng, J. Pan, Y. Zhao, M. Liao, and H. Peng, “Gel Polymer Electrolytes for Electrochemical Energy Storage,” *Adv. Energy Mater.*, vol. 8, no. 7, pp. 1–16, 2018, doi: 10.1002/aenm.201702184.

[20] S. Ramesh and O. P. Ling, “Effect of ethylene carbonate on the ionic conduction in poly(vinylidenefluoride-hexafluoropropylene) based solid polymer electrolytes,” *Polym. Chem.*, vol. 1, no. 5, pp. 702–707, 2010, doi: 10.1039/b9py00244h.

[21] A. M. Stephan, “Review on gel polymer electrolytes for lithium batteries,” *Eur. Polym. J.*, vol. 42, no. 1, pp. 21–42, 2006, doi: 10.1016/j.eurpolymj.2005.09.017.

[22] J. Y. Song, Y. Y. Wang, and C. C. Wan, “- Open Access LibrarySong, J.Y.; Wang, Y.Y.; Wan, C.C. Review of gel-type polymer electrolytes for lithium-ion batteries. J. Power Sources 1999, 77, 183–197, doi:10.1016/S0378-7753(98)00193-1.,” *J. Power Sources*, vol. 77, pp. 183–197, 1999, [Online]. Available: http://www.oalib.com/references/9023829.

[23] Y. Wang and W. H. Zhong, “Development of electrolytes towards achieving safe

and high-performance energy-storage devices: A review," *ChemElectroChem*, vol. 2, no. 1, pp. 22–36, 2015, doi: 10.1002/celc.201402277.

[24] H. S. Choe, B. G. Carroll, D. M. Pasquariello, and K. M. Abraham, "Characterization of Some Polyacrylonitrile-Based Electrolytes," *Chem. Mater.*, vol. 9, no. 1, pp. 369–379, 1997, doi: 10.1021/cm9604120.

[25] E. H. Kil *et al.*, "Imprintable, bendable, and shape-conformable polymer electrolytes for versatile-shaped lithium-ion batteries," *Adv. Mater.*, vol. 25, no. 10, pp. 1395–1400, 2013, doi: 10.1002/adma.201204182.

[26] J. R. Nair, L. Porcarelli, F. Bella, and C. Gerbaldi, "Newly Elaborated Multipurpose Polymer Electrolyte Encompassing RTILs for Smart Energy-Efficient Devices," *ACS Appl. Mater. Interfaces*, vol. 7, no. 23, pp. 12961–12971, 2015, doi: 10.1021/acsami.5b02729.

[27] C. Yang *et al.*, "Flexible Aqueous Li-Ion Battery with High Energy and Power Densities," *Adv. Mater.*, vol. 29, no. 44, pp. 1–8, 2017, doi: 10.1002/adma.201701972.

[28] L. Long, S. Wang, M. Xiao, and Y. Meng, "Polymer electrolytes for lithium polymer batteries," *J. Mater. Chem. A*, vol. 4, no. 26, pp. 10038–10039, 2016, doi: 10.1039/c6ta02621d.

[29] X. Qian, N. Gu, Z. Cheng, X. Yang, E. Wang, and S. Dong, "Plasticizer effect on the ionic conductivity of PEO-based polymer electrolyte," *Mater. Chem. Phys.*, vol. 74, no. 1, pp. 98–103, 2002, doi: 10.1016/S0254-0584(01)00408-4.

[30] W. Liang, Y. Shao, Y. M. Chen, and Y. Zhu, "A 4 v Cathode Compatible, Superionic Conductive Solid Polymer Electrolyte for Solid Lithium Metal Batteries with Long Cycle Life," *ACS Appl. Energy Mater.*, vol. 1, no. 11, pp. 6064–6071, 2018, doi: 10.1021/acsaem.8b01138.

[31] L. Z. Fan, Y. S. Hu, A. J. Bhattacharyya, and J. Maier, "Succinonitrile as a versatile additive for polymer electrolytes," *Adv. Funct. Mater.*, vol. 17, no. 15, pp. 2800–2807, 2007, doi: 10.1002/adfm.200601070.

[32] M. S. Ding, K. Xu, and T. R. Jow, "Conductivity and Viscosity of PC-DEC and PC-EC Solutions of LiBOB," *J. Electrochem. Soc.*, vol. 152, no. 1, p. A132, 2005, doi: 10.1149/1.1833611.

CHAPTER 5. CONCLUSION

In this dissertation, the development of gel polymer electrolyte for safer full cell Li-ion battery fabrication under open-air environment is demonstrated. In chapter 3, GPEs composed of PEGDA polymer host, PC plasticizer, LiTFSI lithium-salt and LiBOB additives are prepared in ambient conditions. Compared to the ionic conductivity of conventional liquid electrolyte (~10^{-3} S/cm), fabricated battery cells exhibit 3.35 x 10^{-3} S/cm ionic conductivity at room. The GPEs function both as a solid-state electrolyte and separator in the full cell configuration of Li-ion coin cells. Due to their chemical stability to moisture and oxygen, LFP cathode and LTO anode, support the development of safer coin-cell batteries that are amenable to assembling in ambient conditions. However, during battery cycling testing, the assembled coin-cell batteries showed rapid capacity fading within 10 cycles. This is caused by the degradation of the gel polymer electrolyte as it is revealed in the LSV test that measure the electrochemical stability window of electrolyte. In chapter 4, the interfacial and electrochemical stability of PEO-based GPEs is enhanced by substituting PEO for PEGDA due to its higher electrochemical stability than PEGDA, that prevented the oxidation of PEO polymer host. In addition, the effect of lithium salts is studied to understand how they affect the cycling stability under ambient conditions, where moisture and oxygen exist. Results show that higher contents of LiBOB improves cycling performance dramatically. Fabricated cells endure 62 cycles with a discharging capacity of ~50 mAh/g. Although discharge capacity needs to be further improved for practical applications, this research opens the door to potential opportunities in the development of safer coin-cells that are amenable to less stringent assembly processes in the open-air.

Overall, this work demonstrates a novel fabrication approach for safer, environmentally friendly, thermally stable, and mechanically robust gel polymer electrolytes for the fabrication of full-cell batteries under open-air and ambient conditions. Future work in further improving electrochemical performance by modifying the chemical and mechanical properties of GPEs has the potential for the development of safer li-ion batteries that are suitable for practical applications.